Odorant receptors tuned to isothiocyanates in *Drosophila melanogaster* are co-opted and expanded in herbivorous relatives

Authors: Teruyuki Matsunaga[1*], Carolina E. Reisenman[2*], Benjamin Goldman-Huertas[3], Srivarsha Rajshekar[2], Hiromu C. Suzuki[2], David Tadres[4], Joshua Wong[5], Matthieu Louis[4], Santiago R. Ramírez[6], Noah K. Whiteman[2, 3*]

Affiliations:

[1] Department of Complexity Science and Engineering, Graduate School of Frontier Sciences, The University of Tokyo, Chiba, Japan

[2] Department of Molecular and Cell Biology, University of California Berkeley, Berkeley, CA

[3] Department of Integrative Biology, University of California Berkeley, Berkeley, CA

[4] Department of Molecular, Cellular, and Developmental Biology, University of California Santa Barbara, Santa Barbara, CA

[5] The Biochemistry, Cellular and Molecular Biology Graduate Program, The Johns Hopkins University School of Medicine

[6] Department of Evolution and Ecology, University of California Davis, Davis, CA

[*]Correspondence to: teru.matsu@edu.k.u-tokyo.ac.jp (T.M.), creisenman@berkeley.edu (C.E.R), and whiteman@berkeley.edu (N.K.W.)

KEY WORDS:

Drosophila melanogaster, olfaction, isothiocyanate, odorant receptor, Or42a, *Scaptomyza flava,* herbivory, evolution, Brassicales, AlphaFold2

ABSTRACT:

Plants release volatile compounds that attract mutualists, deter herbivores, and deceive pollinators. Among them are electrophilic compounds such as isothiocyanates (ITCs) derived Brassicales plants that activate TrpA1 pain receptors by contact in *Drosophila melanogaster* and humans. However, it is unclear whether generalist animals evolved strategies to detect these

electrophilic compounds via olfaction. To address this, and to understand how specialized insects co-opted these toxic compounds as hostplant signatures, we studied generalist micro-feeding (*D. melanogaster* and *Scaptomyza pallida*) and herbivorous mustard specialist drosophilid flies (*S. flava* and *S. montana*). In behavioral assays, *D. melanogaster* exposed to volatile allyl isothiocyanate (AITC) were rapidly immobilized, demonstrating the high toxicity of this compound to non-specialists. Through single sensillum recordings (SSR) from olfactory organs and behavioral assays, we found that the Odorant receptor 42a (Or42a) is necessary for volatile AITC detection and behavioral aversion. RNA expression following heterologous expression showed that lineage-specific, triplicated *S. flava* Or42a proteins exhibited paralog-specific broadened ITC sensitivity. AlphaFold2 modeling followed by site-directed mutagenesis and SSR identified two critical amino acid substitutions that changed Or sensitivity from fruit-derived odors to ITCs during the evolution of *Or42a*. Our findings suggest that ITCs, which are toxic to most insects, can be detected and avoided by non-specialists like *D. melanogaster* through olfaction. In the specialist *S. flava*, paralogous *Or42a* copies experienced gene duplication and amino acid substitutions resulting in expanded ITC sensitivity. Thus, insect olfactory systems can rapidly adapt to toxic host plant niches through co-option of chemosensory capabilities already present in their ancestors.

INTRODUCTION:

Plants have evolved the ability to synthesize a diverse array of potentially toxic specialized metabolites that can provide resistance against insect herbivory. In turn, herbivorous insects have evolved diverse morphological, physiological, and behavioral counter-strategies to avoid these chemicals if encountered, or to mitigate their effects if ingested (Mithöfer and Boland 2012). Some herbivores even co-opt these plant toxins as oviposition or feeding stimulants and chemical defenses of their own. For example, monarch butterfly (*Danaus plexippus*) larvae evolved target site insensitivity in the sodium potassium ATPase against the cardenolides released from milkweed (*Asclepias* spp.) host plants upon wounding (Dobler et al. 2012). The caterpillars sequester these heart poisons, which serve as effective defenses against predation throughout the life of the insect (Reichstein et al. 1968). Although cardenolides have one major molecular target in insects, many plant toxins are far more promiscuous in their modes of action, which presents a different "evolutionary hurdle" (Southwood 1972) to herbivores. Among them are various alkaloids, terpenes, and green leaf volatiles (GLVs) electrophilic compounds,

60 such as piperine from black pepper, caryophyllene from cloves, and *trans*-2-hexenal from a wide range
61 of leaves and grasses (Noge and Becerra 2015; Yaffe et al. 2015; Iorio et al. 2022). These compounds
62 intoxicate or deter herbivores and pathogens by interacting with nucleophilic sites in biological
63 molecules, rendering them toxic or inhibitory (War et al. 2012).

64 Brassicales plants that include mustards (Brassicaeae) have evolved a sophisticated chemical
65 defense system that produces promiscuous electrophilic toxins (Ahuja et al. 2010). These plants produce
66 non-toxic glucosinolates from various amino acid precursors, some of which are hydrolyzed *in planta* to
67 form toxic compounds that can include electrophilic isothiocyanates (ITCs) (Hopkins et al. 2009). ITCs
68 are defined by a R−N=C=S functional group wherein the carbon is attacked by nucleophiles such as the
69 sulfhydryl groups of cysteines. For example, allyl isothiocyanate (AITC) is derived from radish
70 [*Raphanus sativus* (Cuellar-Nuñez et al. 2022)], while butyl isothiocyanate (BITC) and other ITCs
71 bearing similar structures are derived from cabbage [*Brassica oleracea* (MacLeod et al. 1989)]. The
72 chemical diversity of glucosinolates allows Brassicales plants to effectively deter a wide array of
73 herbivorous insects because different species have different mixtures of glucosinolates, making it more
74 difficult for insects to adapt (Winde and Wittstock 2011).

75 One herbivorous insect lineage that has evolved to cope with more promiscuous toxic plant
76 metabolites like ITCs are obligated leaf-mining drosophilid flies in the genus *Scaptomyza* (e.g., *S. flava*
77 and *S. montana*: hereafter *Sfla* and *Smon,* respectively) which are specialized primarily on Brassicales
78 plants. *Sfla* likely has a broader host range, as it can be reared on plants from other lineages in addition
79 to Brassicales, such as Fabaceae or even Caryophyllaceae in New Zealand (Martin 2004; Maca 1972),
80 whereas *Smon* appears to be more restricted to Brassicaceae within the Brassicales and may require
81 plants that produce indolic glucosinolates specifically (Gloss et al. 2017). *Scaptomyza* species form a
82 clade that is phylogenetically nested within the paraphyletic *Drosophila* subgenus. Gloss et al. (2014)
83 found that yeast-feeding *Drosophila melanogaster* (hereafter *Dmel*) uses promiscuous glutathione *S*-
84 transferases (GSTs) in the gut to detoxify dietary ITCs released from glucosinolate-bearing Brassicales
85 plants like thale cress (*Arabidopsis thaliana*), broccoli (*Brassica oleracea*) and wasabi (*Eutrema*
86 *japonicum*). Further, they characterized a set of *Scaptomyza*-specific GSTs that experienced rapid gene
87 duplication and non-synonymous changes during the evolution of herbivory, resulting in among the
88 most efficient GSTs known from animals in detoxifying ITCs (Gloss et al. 2014; Gloss et al. 2019).
89 Additionally, Brassicales-feeding *Scaptomyza* flies may minimize their exposure to glucosinolate-

90 derived toxins by selectively ovipositing on leaves that contain lower glucosinolate concentrations
91 (Humphrey et al. 2016).

92 Insects can behaviorally avoid toxic chemicals through gustation and/or olfaction (e.g. Bernays
93 and Chapman 1987; Stensmyr et al. 2012; Scott 2018; Chen and Dahanukar 2020; Dweck and Carlson
94 2020). In *Dmel*, physical contact of ITCs by the tarsi and/or proboscis induces behavioral aversion
95 through gustatory receptor cells that express the nociceptive "wasabi receptor" TrpA1 and Painless (Al-
96 Anzi et al. 2006; Kang et al. 2010; Kim et al. 2010; Mandel et al. 2018). Volatile exposure to extracts
97 containing phenethyl isothiocyanate (PITC) from turnip or rutabaga kills *Dmel*, suggesting that volatile
98 PITC is toxic to these insects at biologically meaningful concentrations (Lichtenstein et al. 1964). In
99 addition, volatile allyl isothiocyanate (AITC) causes behavioral aversion in fire ants (*Solenopsis invicta*)
100 (Hashimoto et al. 2019). All these findings raise the possibility that insects have evolved olfactory
101 sensory neurons (OSNs) that detect plant-derived electrophilic compounds such as ITCs, leading to
102 olfactory-mediated behavioral avoidance in generalists, as has been found in the gustatory system.

103 *Scaptomyza* includes species that are both non-herbivorous (e.g., microbe-feeding) and
104 herbivorous (Aguilar et al. 2024). However, the most recent common ancestor of the herbivores is
105 hypothesized to have been microbe-feeding based on ancestral state reconstruction (Whiteman et al.
106 2011; Whiteman et al. 2012; Peláez et al. 2023). Of particular interest are the Brassicales plant
107 specialists *Sfla* and *Smon*, which are closely related species in the exclusively herbivorous subgenus
108 *Scaptomyza* of the genus *Scaptomyza* (Kim et al. 2021). Additionally *Or85d, Or42b, Or9a* and *Or22a,*
109 which in *Dmel* mediate the olfactory detection of fermentation products of brewer's yeast and other
110 microbes, were lost in a stepwise fashion during the evolution of herbivory in *Scaptomyza* (Goldman-
111 Huertas et al. 2015). Furthermore, the *Sfla* paralogs of the antennal odorant receptor Or67b, which in
112 *Dmel* is encoded by a single *Or67b* copy and responds to green leaf volatiles such as *trans*-3-hexenol,
113 respond to a subset of ITCs only in *Sfla*, not *Dmel* (Matsunaga et al. 2021). Although there has been
114 some progress, whether and to what extent generalist insects avoid volatile electrophilic compounds like
115 ITCs on the one hand, and how evolution has reshaped the sensory receptors of specialists to facilitate
116 aversion and/or attraction on the other, is still largely unknown, yet is a central problem in understanding
117 how organisms invade toxic niches and host herbivorous insects specialize on toxic host plants.

118 We addressed this problem in *Dmel* and a set of *Scaptomyza* spp. exhibiting a gradient in
119 microbe-feeding and plant-feeding habits. We first recapitulated the experiments of Lichtenstein et al.

120 (1964) with the more commonly used AITC instead, and found that *Dmel* is rapidly immobilized (likely
121 intoxicated) by exposure to moderate concentrations of volatile AITC. This indicates that *Dmel* may
122 have evolved odorant receptors that respond to and release aversive behaviors toward volatile ITCs. We
123 found that Or42a, which is expressed specifically in *Dmel* maxillary palp basiconic sensilla 1a (pb1a)
124 OSNs (Ray et al. 2007), is highly sensitive to volatile AITC and is necessary for behavioral aversion to
125 this compound. We discovered that the mustard plant specialist *Scaptomyza* species *Sfla* and *Smon*, but
126 not microbe-feeding *Scaptomyza* and *Dmel*, have expanded their ITC sensitivity range. In *Sfla*, this was
127 coupled with a concomitant increase in the number of *Or42a*-positive-OSNs, and with a triplication of
128 the *Or42a* gene. We then used site directed mutagenesis and found that via just two amino acid
129 substitutions, one of these Or42a paralogs in *Sfla* switched its sensitivity from odors that activate the
130 Or42a of microbe feeders to odors that activate mustard specialists, paralleling the niche shift of the
131 mustard-feeding *Scaptomyza*. Taken together, these results illustrate how plant-derived volatile toxins
132 like electrophilic ITCs can negatively impact insect behavior and fitness, how the insect olfactory
133 system detects them leading to behavioral avoidance, and how host-plant specialization reshapes the
134 organization and molecular function of toxin-detecting Ors.

135

136 **MATERIAL AND METHODS:**

137 **Fly Husbandry**

138 Microbe-feeding *Dmel* was reared on cornmeal medium. Microbe-feeding *S. pallida* (hereafter:
139 *Spal,* subgenus *Parascaptomyza*) and *S. hsui* (hereafter: *Shsu,* subgenus *Hemiscaptomyza*) were reared
140 in vials of cornmeal molasses media covered with a mixture of Carolina biological supply instant
141 *Drosophila* media (Burlington, NC) mixed with blended spinach leaves, and then covered with a layer
142 of defrosted frozen spinach leaves. The obligate leaf-miners *Sfla* and *Smon* (subgenus *Scaptomyza*) were
143 cultivated on potted fresh laboratory-grown *Arabidopsis thaliana* Col-0. Isofemale lines of microbe
144 feeding *Shsu* and *Spal*, as well as the herbivorous *Smon,* were collected along Strawberry Creek on the
145 UC-Berkeley Campus in Berkeley, California, USA (Kim et al. 2021), and a line of *Sfla* was collected
146 from a meadow near Dover, New Hampshire, USA. All species were kept at 23±2°C and 60% relative
147 humidity in a 10L:14D light cycle under fluorescent lights. The following lines (stock #) were obtained
148 from the Bloomington *Drosophila* Stock Center: *Or42a-/-* (60821), *Or42a-Gal4* (9970), w^{1118} (3605),
149 $TrpA1^{1}$ (26504), *Or35a-/-* (91811) *Or7a-/-* (91811), and a genetic background control for the three Or

150 null mutant lines (68384). The *Or35a-/-* line (10564) was obtained from the Korea Stock Center. The
151 *Or67d*^{Gal4} line was a gift from the laboratory of Barry J. Dickson.

152

153 **Single sensillum recordings (SSRs)**

154 One-five days old fed female flies were prepared for SSR as described in Matsunaga et al.
155 (2021). Briefly, a silicon tube delivering a constant flow of charcoal-filtered air (16 ml/min, measured
156 using a flowmeter, Gilmont Instruments, USA) was placed near the fly's head capsule, and the tip of the
157 stimulation pipette (50 ml) was inserted into the constant air stream. The stimulation pipette contained a
158 0.5 cm x 5 cm piece of filter paper loaded with 20 µl of an odorant solution or the solvent control. A
159 pulse of clean air (duration = 1 sec) was delivered to the stimulus pipette using a membrane pump
160 operated by a Stimulus Controller CS 55 (Syntech, Buchenbach, Germany). Sensilla identification was
161 conducted using the following diagnostic odorants (as described in Dweck et al. 2016; Gonzalez et al.
162 2016), all >95% pure (Sigma-Aldrich, St. Louis, MO, USA): ethyl acetate (CAS# 141-78-6) for
163 identifying *Dmel* pb1a; AITC (CAS # 57-06-7) for identifying *Scaptomyza* pb1a-like olfactory sensory
164 neurons (OSNs); 4-ethylguaiacol (CAS# 2785-89-9) for identifying *Dmel* and *Scaptomyza* pb1b-like
165 OSNs; fenchone (CAS# 1195-79-5) for identifying *Dmel* and *Scaptomyza* pb2a OSNs; guaiacol
166 (CAS# 90-05-1) for identifying *Dmel* and *Scaptomyza* pb2b OSNs; phenethyl acetate (CAS# 103-45-7)
167 for identifying *Dmel* pb3b, *Sfla* pb3b, and *Smon* pb3a-like OSNs; and 2-heptanone for identifying *Shsu*
168 and *Spal* pb3a-like OSNs. All odorants were diluted in mineral oil (CAS# 8042-47-5) except γ-
169 hexalactone (CAS # 695-06-7), which was diluted in dimethyl sulfoxide (DMSO, CAS# 67-68-5)
170 because it did not dissolve completely in mineral oil and sometimes produced response artifacts.
171 Odorants were diluted to 1:100 vol/vol for stimulation unless otherwise noted. Supplementary file 1 lists
172 all the chemicals used in this study.

173 The "net number of spikes/second" was obtained by counting the number of spikes originating
174 from the OSN of interest within a 0.5-second timeframe which started 0.2 seconds after the onset of
175 stimulation. This count was then adjusted by subtracting the background spiking activity (# of spikes
176 within a 0.5 second interval preceding the onset of the stimulation), and then doubled to represent the
177 number of spikes/second. In all figures, unless otherwise stated, we represent the "control-subtracted net
178 # of spikes/sec" to odorant stimulation, calculated by subtracting the average net # of spikes/sec in
179 response to the solvent control (mineral oil or DMSO) from the net # of spikes/sec evoked by each

odorant stimulation. Control-subtracted spike data are compiled in Supplementary file 2. The Butyl-ITC (BITC) to γ-hexalactone spike ratio (Figure 4F and Figure Supplement 11) was calculated as: net # of spikes/sec evoked by BITC / (net # of spikes/sec evoked by BITC + net # of spikes/sec evoked by γ-hexalactone). We used this denominator for the ratio because the control-subtracted net # of spikes upon γ-hexalactone stimulation occasionally produced negative values (likely a response to the solvent control).

Half maximal effective concentrations (EC_{50}) were calculated using *Quest Graph™ EC50 Calculator.* (AAT Bioquest, Inc., 4 Mar. 2025, https://www.aatbio.com/tools/ec50-calculator). We primarily used the two-parameter feature with normalization, where responses were normalized to the largest response within the same chemical-species pair, with the minimum set to 0. This approach was chosen because the lowest tested concentration (10^{-5}) still elicited non-zero spike activity (>10) in some chemical-species pairs. The four-parameter method without normalization, in which the maximum and minimum responses were free parameters, was used in cases where the two-parameter method failed to fit a logistic regression (summarized in Supplementary file 2) or when analyzing sec-Butyl ITC (SBITC) data. For SBITC, the four-parameter method was necessary because the highest tested concentration (10^{-2}) did not reach saturation (<100 spikes). When both the two-parameter and four parameter methods failed due to lack of convergence at the lowest concentration (10^{-5}), resulting in a calculated value of 0, we instead used the minimum value observed within that chemical-species group.

The *Or67d*^{GAL4} line was used to generate flies expressing *Or42a* homologs in the at1 "empty neuron" system, as described in (Kurtovic et al. 2007).

The spike amplitude differences between the two types of OSNs housed in pb3a and pb3b were less distinct in *Scaptomyza*, and therefore we could not completely rule out the possibility that we occasionally erroneously assigned spiking to each of these two OSNs types.

Immobility assay

To investigate the effect of AITC volatiles in wild-type *Dmel* (Canton-S strain), we used a 9 cm diameter plastic petri dish (Nunc, Denmark) with a piece of fabric mesh placed horizontally between the base and the lid, creating two chambers (Figure Supplement 1A). The upper chamber housed 8-10 male flies 3-5 days old, and the lower chamber contained four 5 µl drops of the odor solution (or the solvent

control) evenly dispersed. Because the mesh prevented the flies from reaching the bottom chamber, insects were exposed to the volatile chemicals but could not directly contact (i.e. taste) the odor solution, unless the molecules adhered to the walls of the chamber after volatilizing. After each test started, we counted the number of mobile flies every 10 minutes up to one hour and calculated the percentage of mobile flies at each time point. Flies exhibiting no movement for >30 seconds were likely intoxicated. AITC or γ-hexalactone were diluted in either mineral oil or DMSO at various concentrations. Mobility data analysis was performed using the log-rank (Mantel-Cox) test (Mantel 1966). The complete immobility assay dataset is compiled in Supplementary file 3.

Consumption assay

Groups of 2-4 days old mated female flies (n=11-15) were wet-starved for 24 hours, and then transferred to a vial containing a piece of filter paper (2.7 cm diameter, Whatman, cat. No 1001 125) impregnated with 160 µl of 50 mM D-glucose (Sigma-Aldrich, USA) dyed blue with Erioglaucine (0.25 mg/ml, Sigma-Aldrich, St. Louis, MO, USA) (Reisenman and Scott 2019) (Figure Supplement 1B). Flies were allowed to feed for 15 minutes (10 minutes in tests with γ-hexalactone), vials were frozen (>60 minutes), and the amount of blue dye in the flies' abdomen was scored blind to treatment (see below). The odor source consisted of a strip of filter paper (0.25 cm wide x 1.5 cm long) impregnated with either 10 µl of an odorant solution (test) or 10 µl of the solvent (control), which was placed inside a container (1.3 cm long x 0.75 cm diameter) with a meshed bottom affixed to the vial's flug (Figure Supplement 1B). This allowed diffusion of odors into the fly vial but prevented flies from contacting the odor source. Control tests, with vials containing food solution but only the solvent control inside the meshed container, were conducted in parallel with experimental tests to control for fly cohort and day-to-day variability.

Food consumption was estimated by scoring individual flies in each vial blind to treatment using the following five-point scale (Reisenman and Scott 2019): 0 (no dye = no food), 0.25 ("trace" of blue dye), 0.5 (up to ¼ of the abdomen dyed blue), 1 (more than ¼ but less than ½ of the abdomen dyed blue), and 2 (more than ½ of the abdomen dyed blue). For each vial, a single feeding score value was calculated as: $[(0 \times n_0 + 0.25 \times n_{0.25} + 0.5 \times n_{0.5} + 1 \times n_1 + 2 \times n_2) / N]$, where $n_{(0\text{-}2)}$ denotes the number of flies in each score category, and N the total number of flies/vial. Feeding scores from each test vial (flies tested in presence of odor) were normalized to the averaged feeding score of control vials (flies of the same genotype tested in absence of odor) assayed on the same day. Normalized feeding scores for each

genotype and odor were compared against the null hypothesis (median feeding score = 1) using one sample signed rank tests. That is, medians not different from 1 indicate that the odorant did not reduce neither enhanced consumption, while medians significantly less than 1 or more than 1 respectively indicate feeding aversion or enhancement. Normalized data from control and mutant flies were compared using Mann-Whitney U tests. In all cases results were considered statistically significant if $p<0.05$. The consumption assay data is compiled in Supplementary file 4.

Positional olfactory assay

To study the olfactory orientation of insects towards odors, we conducted assays with non-starved 3-4 days old mated females (Figure Supplement 1C). Flies (n=10-12/test) were anesthetized on ice (5-7 minutes) and placed in a small piece of clear Tygon tube, capped in both sides with a conical PCR plastic Eppendorf. After another about 4-5 minutes, the Tygon tube with the anesthetized flies was uncapped and connected to the cut ends of two glass Pasteur pipettes and the assay started; flies usually resumed activity after about 3-4 minutes. Each of the two opposite ends of the pipettes were respectively connected (via a small piece of Tygon tube) to a 1.75-ml glass vial containing 10 µl of the odor solution (AITC 1: 500 vol/vol, or γ-hexalactone 1:100 or 1:10 vol/vol) or 10 µl of the control solvent (mineral oil, or DMSO). Tests with apple cider vinegar used 30 µl instead, and water was used as a control. The distal ends of the pipettes were separated from the glass vials with a small piece of fabric mesh, which allowed the odorant to diffuse into the pipette while also preventing insects from contacting the odor source (Figure Supplement 1C). The odor and control sides were switched between assays. Assays were conducted on a white surface under white light at 21-24 °C, about 2-6 hours after lights on. Once each assay started, the number of flies in the pipette closest to the vial with the odor (referred to as "odor side" or "odorous tube" for simplicity), in the pipette closest to the vial with the solvent control ("control" side/tube), and in the Tygon tube that connected both pipettes (release site) were counted every 5 minutes until minute 35, and then again at 65 minutes in the case of tests with AITC. For each assay, we calculated the % of insects that made a choice for one or the other tube as: [(#of insects in the odor side + # of insects in the control side) / total number of insects released)] x 100. The percentage of insects that choose the odorous tube was calculated based on the total number of insects that made a choice as: [# of insects in the odor side / (# of insects in the odor side + # of insects in the control side)] x 100. Assays in which less than 40% of insects made a choice for either side at all time points were discarded (<5% of assays). For each fly genotype and odorant, the % of insects that choose the odor side

271 at each time point was compared against the median value expected under the hypothesis that insects
272 distributed at random between the two tubes (50% of insects in each tube) using one-sample signed rank
273 tests. Thus, we assessed whether the insects significantly avoid the odorous tube (if median<50%),
274 prefer it (if median>50%), or showed a random preference. Also, at each time point and for each odor
275 (and concentration when applicable), the responses of the null mutants (*Or42a-/-*, *Or7a-/-* and *Or35a-/-*)
276 and their genetic background control (listed above) were compared via Mann-Whitney U tests. In all
277 cases results were considered significant if $p<0.05$. In most cases we used two-tailed tests (e.g. for
278 testing $median_1 \neq median_2$), but in a few cases we used one-tailed tests (e.g. for testing $median_1 >$
279 $median_2$ or $median_1<median_2$, Figure Supplement 2G-I). The positional olfactory assay data is included
280 in Supplementary file 5.
281

282 **RNA-sequencing of maxillary palps**

283 Newly emerged adults of *Sfla* and *Spal* were collected from our colony and kept in humidified
284 vials with 10% honey water until dissection, to minimize potential differences in nutrition resulting from
285 differences in the two species' larval diet. Three to ten days old flies were anesthetized with CO_2, and
286 their maxillary palps were hand-dissected using forceps. Approximately 100-120 flies were pooled for a
287 single sample. The dissected tissues were directly collected in LB+TGA lysis buffer from Reliaprep
288 RNA Tissue Miniprep System (Promega, USA), and homogenized using a Biomasher Standard
289 homogenizer (Takara Bio Inc., USA) in a dry ice ethanol bath. The sample lysates were stored at -80°C
290 until RNA extraction. Total RNAs were extracted from the lysates using ReliaPrep RNA Tissue
291 Miniprep System (Promega, USA) according to the manufacturer's protocol, and quantified using a
292 Qubit RNA High Sensitivity kit (Thermo Fisher Scientific, USA). Library preparation was performed at
293 the Functional Genomics Laboratory (FGL) at UC Berkeley. Due to the low yields of our maxillary
294 palp-derived total RNAs, cDNA libraries were first produced by Takara SMART-Seq mRNA Ultra-low
295 input RNA kit (Takara Bio Inc., USA) with 8 cycles of PCR for the amplification, and then processed by
296 KAPA HyperPrep kit for DNA (Roche Sequencing, USA) with 9 cycles of PCR for attaching in-house
297 sequencing adapters and index primers. cDNA libraries were then sequenced on an Illumina NovaSeq
298 6000 150 PE S4 flowcell, targeting 25M read pairs per library by the UC Berkeley Vincent J. Coates
299 Genomics Sequencing Laboratory. For read mapping, we used previously reported reference genome
300 assemblies and gene annotations from *Sfla* (Peláez et al. 2023) and *Spal* (Kim et al. 2021) for subsequent
301 bioinformatic analyses. Raw RNA-seq reads were filtered using Fastp v0.21.0 (Chen et al. 2018) and

302 mapped to the respective reference genomes using STAR v2.7.1a (Dobin et al. 2013) to generate
303 multiple alignment (BAM) files, which were then converted to read count data using HTseq v0.9.1
304 (Anders et al. 2015). Count data for the Or gene family were converted to RPM (reads per million;
305 Supplementary file 6).
306

307 **HCR RNA FISH**

308 One-to-four-days-old female *Sfla* and *Spal* were collected and anesthetized with CO_2. Whole
309 mouthparts were removed and immediately placed in 2 mL of fixative (4% vol/vol paraformaldehyde in
310 1x phosphate buffered saline with 3% vol/vol Triton X-100 added, PBST) in LoBind Eppendorf tubes,
311 and fixed for 22 hours at 4°C on a nutator.

312 Fixative was removed and replaced with 2 mL of cold (4°C) 3% PBST, and tubes were agitated
313 on a nutator for 5 minutes. This step was repeated once more and then again with cold 0.1% PBST; samples
314 were then washed with 1 mL of cold 0.1% PBST 4 times and agitated on a nutator (5 min/wash). PBST
315 was removed and replaced with 300 µL of warm (37°C) HCR RNA FISH probe hybridization buffer
316 (Molecular Instruments, Inc., Los Angeles, CA) and incubated for 30 minutes. The probe hybridization
317 solution was prepared by adding 5µL of 1µM of probe B1-*Spal Or42a* and probe B2-*Spal Orco* (or probe
318 B1-*Sfla Or42a* and probe B2-*Sfla Orco*) to 300 µL of pre-heated probe hybridization buffer for the *Spal*
319 or the *Sfla* tissues and kept at 37°C. Finally, the buffer was replaced with preincubated probes in
320 hybridization buffer and kept at 37°C for 22 hours.

321 Samples were next washed 3 times with 500 µL of preheated (37°C) probe wash buffer for 5 min
322 on a heating block. Ten µL of 3µM amplification hairpins one and two of b1-488 and b2-637 HCR
323 amplifiers (Molecular Instruments, Inc., Los Angeles, CA) were snap cooled on a thermocycler at 95°C
324 for 90 secs and then at 20°C for 30 min, and covered with aluminum foil to prevent fading. Samples were
325 kept at room temperature and washed 3 times with 500 µL of 0.75M NaCl, 75mM sodium citrate and
326 0.1% Tween-20 vol/vol (SSCT) for 5 minutes, and then incubated in 500 µL amplification buffer
327 (Molecular Instruments, Inc., Los Angeles, CA) for 30 minutes. Snap cooled hairpins were added to two
328 vials containing 300 µL of amplification buffer for each species. The amplification buffer was removed
329 from the vials and replaced with the hairpin solution; tubes were covered in aluminum foil and incubated
330 at room temperature for 22 hours.

331 Samples were washed twice with 500 µL of SSCT solution for 5 minutes, twice for 30 minutes,
332 and finally washed again for 5 minutes. Samples were then stained with 300 nM DAPI stain in 0.1% PBST

333 for 15 minutes and then washed 3 times with 0.1% PBST for 5 minutes. Tissues were transferred to a
334 microscope slide and mounted in a drop of ProLong diamond antifade mounting (Life Technologies Corp.,
335 Eugene, OR) and stored at 4°C until examination. Confocal imaging of fixed samples was performed
336 using a Zeiss LSM 880 microscope in the AiryScan mode. Raw images were processed using Zeiss ZEN
337 Black software. Orco-positive cells (visualized with the 488 nm laser) and Or42a-positive cells (visualized
338 with the 633 nm laser) were manually counted using the "Cell Counter" plugin in Fiji (ImageJ) software.
339 Supplementary file 7 contains cell counts of RNA FISH.

340

341 ***Scaptomyza Or42a* gene cloning and generation of *UAS* lines**

342 RNA was isolated from 15-25 days laboratory-reared adults of both sexes of *Spal* and *Sfla* using
343 the ReliaPrep Miniprep system (Promega, W.I., USA). Complementary DNA (cDNA) was synthesized
344 using the qScript cDNA Supermix (Quantabio, Beverly, MA, USA). The paralogs were amplified via
345 touchdown PCR, using primers that target the highly variable regions of the 5' and 3' untranslated
346 regions (UTRs). The single *Or42a2* gene of *Spal* was amplified using touchdown PCR with primers
347 targeting the coding region (Q5 DNA Polymerase, #M0491, NEB) (Supplementary file 8). All PCR
348 products underwent gel purification (11-300C, Zymo Research) and were subsequently cloned using the
349 Gibson Assembly (E2611S, NEB) following the manufacturer's instructions into the UAST-attB vector
350 (DGRC Stock 1419; RRID:DGRC1419, Bischof et al. 2007). The ligation products were transformed
351 into DH5α competent cells (T3007, Zymo Research). After confirming the sequences using Sanger
352 sequencing, the 5' and 3' UTRs of the plasmids containing the *Sfla Or42a* paralogs were removed. This
353 was achieved by first amplifying the coding region using PCR, followed by gel purification and ligation
354 back into UAST-attB vector via Gibson Assembly. The resultant plasmids were Sanger sequence-
355 verified. Finally, these plasmids were microinjected into the attP40 site (P{nos-phiC31\int.NLS}X,
356 P{CaryP}attP40, line # 25709, Rainbowgene) to create transgenic lines for *Spal Or42a*, *Sfla Or42a2*,
357 *Sfla Or42a3* and *Sfla Or42a4*. All lines were confirmed by sequencing prior to experiments.

358 **Screen of candidate amino acids using AlphaFold2 3D structural prediction**

359 CDS of *Sfla Or42a3* and *Sfla Or42a4* were confirmed by palp RNAseq data using IGV_2.16.0.
360 CDSs of *Sfla Or42a3* and *Sfla Or42a4* were then used as inputs into ColabFold (Jumper et al. 2021;
361 Mirdita et al. 2022). Then the output models ranked first (rank1) were selected, visualized, and 3D-

362 aligned by using PyMol2.5.3. We focused on the regions where predicted Local Distance Difference
363 Test (pLDDT) scores exceed 70, as structures with lower pLDDT scores are often unreliable (Mariani et
364 al. 2013). We focused on the S5-S6 transmembrane helices because previous studies suggested that the
365 binding pockets of odorant receptors are located in the transmembrane region (Butterwick et al. 2018;
366 Del Mármol et al. 2021; Zhao et al. 2024), and our amino acid alignment of *Sfla* Or42a3 and *Sfla*
367 Or42a4 provided the highest root mean square deviation (RMSD) scores in this region. In silico
368 substitutions of amino acids were performed individually on *Sfla* Or42a3, and the resulting sequences
369 were then re-input into ColabFold, the model with rank1 was selected, and the structures were 3D-
370 aligned with that of *Sfla* Or42a4. This process of in silico mutation and alignment was repeated until the
371 RMSD scores for the S5-S6 region were reduced to a value comparable to the other region (~0.1 Å). All
372 pdb files used in this study are included in Supplementary file 9.

373

374 **Site-directed mutagenesis**

375 Conventional PCR was conducted using plasmids of *Sfla Or42a3* as backbone (Q5 DNA
376 polymerase, #M0491, NEB; Supplemental File 1). Primers were designed to introduce the point
377 mutations (Supplementary file 1). The PCR product underwent gel purification (11-300C, Zymo
378 Research) and the methylated plasmids were digested with DpnI for 1 hour at 37℃ (QuickChange,
379 Agilient Technology, USA). Ligation was performed by incubation at 16℃ for 30 minutes (DNA
380 ligation kit Mighty mix, Takara, Japan) and the products were transformed into DH5α competent cells
381 (Takara, Japan). After confirming the sequence using Sanger sequencing, the plasmid was microinjected
382 into the attP40 site (P{nos-phiC31\int.NLS}X, P{CaryP}attP40, line # 25709, Rainbowgene) to create
383 transgenic A181D S307P fly. The line was confirmed by sequencing prior to experiments.

384

385 **RESULTS**

386 **Volatile AITC rapidly immobilizes *Dmel***

387 We conducted mobility assays as a proxy for toxicity with various concentrations of volatile
388 AITC (from 1:500 to 1:2.5 vol/vol). In our experimental setup, a fabric mesh separated the chamber
389 containing the flies from the chamber containing the AITC solution (Figure Supplement 1A) and
390 therefore, flies were exposed to volatile AITC but could not contact (i.e. taste) the AITC solution

391 directly. While all animals in both the control treatment and those exposed to AITC 1:250 and 1:500
392 vol/vol remained active, most flies exposed to AITC concentrations ≥ 1:50 vol/vol became paralyzed
393 (likely highly intoxicated or even dead) within 10 minutes (Figure 1A). Thus, this rapid immobilization
394 indicates that plant-derived electrophilic compounds like AITC can have a strong negative effect on
395 flies, consistent with previous findings using volatile PITC (Lichtenstein et al. 1964).

396

397 **Volatile AITC is detected by Or42a in *Dmel***

398 The high toxicity caused by volatile AITC indicates that this volatile had the potential to be
399 detected by the fly's olfactory system, and that this could provide a fitness benefit if these volatile toxins
400 were then behaviorally avoided. To investigate this, we conducted exhaustive single sensillum
401 recordings (SSR) from the fly's olfactory organs, the antennae and the maxillary palps, upon stimulation
402 with volatile AITC. Several OSNs showed excitatory responses to AITC, but OSNs in palp basiconic
403 (pb) sensilla (pb1a) were the most strongly activated (Figure 1 B-C, >100 spikes/sec). Because previous
404 studies reported that *Dmel* pb1a OSNs express Or42a (Couto et al. 2005), we investigated whether AITC
405 responses in pb1a OSNs are indeed mediated by Or42a. OSNs in pb1 sensilla from control flies showed
406 strong responses to volatile AITC, while OSNs in pb1 sensilla from *Or42a* null mutant flies showed no
407 response (Figure 1D, <2 spikes/second), indicating that Or42a detects volatile AITC in these sensilla.
408 Furthermore, OSNs in pb1a of *TrpA1* null mutant flies responded strongly to AITC (>150
409 spikes/second, Figure 1D), showing that the contact chemoreceptor TrpA1 is not necessary for maxillary
410 palp olfactory detection of this compound. Or42a is the first Or reported to detect an ITC in *Dmel* to our
411 knowledge.

412

413 **Volatile AITC repels *Dmel* via Or42a**

414 Next, we examined if activation of OSNs housing Or42a plays a role at the behavioral level
415 (whole organism). Previous studies have shown that the presence of food-related odorants increases
416 sugar consumption in *Dmel* (Reisenman and Scott, 2019). Based on this, we hypothesized that the
417 presence of aversive odorants such as AITC would decrease sugar consumption. We conducted
418 consumption assays in which groups of 10-15 food-deprived female flies were offered 50 mM glucose
419 water solution dyed blue in the presence or absence of volatile AITC (1:500 vol/vol loaded on filter
420 paper), such as that flies could smell, but not contact, the AITC solution (Figure Supplement 1B). After

Figure 1

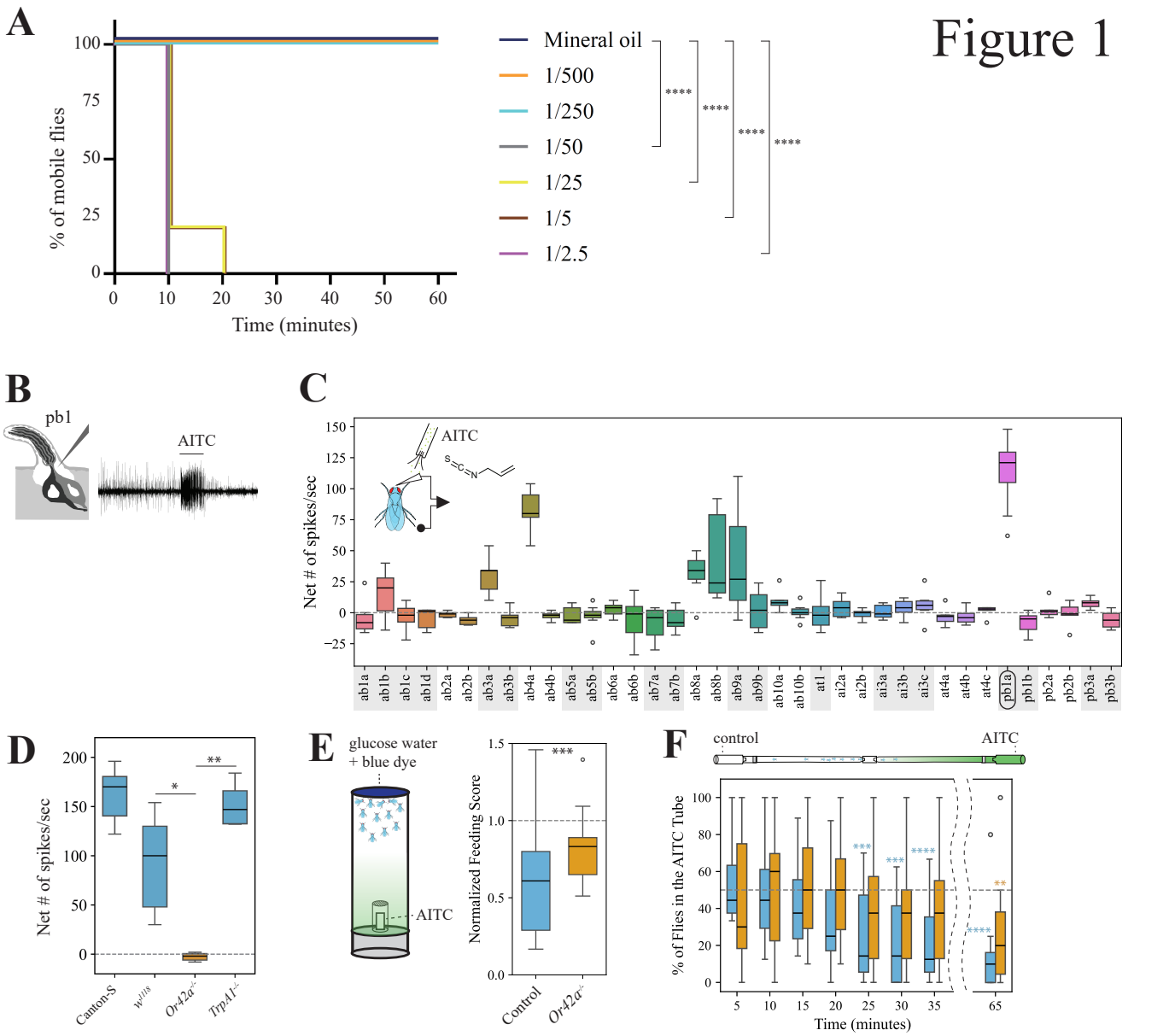
A
% of mobile flies
Time (minutes)
Mineral oil
1/500
1/250
1/50
1/25
1/5
1/2.5
****
B
pb1
AITC
C
Net # of spikes/sec
AITC
ab1a ab1b ab1c ab1d ab2a ab2b ab3a ab3b ab4a ab4b ab5a ab5b ab6a ab6b ab7a ab7b ab8a ab8b ab9a ab9b ab10a ab10b at1 ai2a ai2b ai3a ai3b ai3c at4a at4b at4c pb1a pb1b pb2a pb2b pb3a pb3b
D
Net # of spikes/sec
Canton-S
Or42a
Trpa1
E
glucose water
+ blue dye
AITC
Normalized Feeding Score
Control
Or42a
F
control
AITC
% of Flies in the AITC Tube
Time (minutes)

421 15 minutes flies were frozen and then a single feeding score/vial was calculated based on the amount of
422 blue dye in the abdomen of all flies within a vial. We found that genetic background control flies fed
423 less when volatile AITC was present than in the presence of the solvent control (one-sample signed rank
424 tests on normalized data, $p<0.001$, $n=16$; Figure 1E); wild-type Canton-S flies also fed less in presence
425 than in absence of volatile AITC ($p<0.05$, $n=23$; not shown). Mutant flies fed less in the presence of
426 AITC volatiles ($p<0.05$) as well, but their feeding scores were higher than that of the genetic control
427 group ($p<0.001$, Mann-Whitney U test; Figure 1E). These results indicate that Or42a mediates aversion
428 to AITC in this behavioral context.

429 Additionally, we conducted a positional olfactory assay based on Ohashi and Sakai (2015), with
430 various modifications to prevent flies from physically contacting the odor source (Figure Supplement
431 1C). Groups of 10-12 female flies were released at the juncture between the two glass pipettes and were
432 allowed to choose between the pipette closest to the odor source ("odorous side/tube") and the pipette
433 closest to the solvent ("control side/odorless tube"; Figure Supplement 1C). The number of flies in each
434 tube as well as in the release section was counted every five minutes up to minute 35, and then again at
435 65 minutes. We first confirmed that flies can show normal olfactory-guided behavior in this behavioral
436 set-up using apple cider vinegar, a well-established olfactory attractant (Semmelhack and Wang 2009;
437 Becher et al. 2010). Canton-S flies preferred the odorous tube from minute 25 onwards (one-sample
438 signed rank tests, $p<0.05$ in all cases, $n=21$, Supplementary File 5). We then tested whether AITC causes
439 olfactory repellence in this behavioral context. Genetic control flies and wild-type Canton-S flies
440 avoided the AITC tube at various time points (25, 30, 35 and 65 minutes in genetic controls, Figure 1F;
441 and from 25 minutes onwards in Canton-S, Figure Supplement 2B). In contrast, *Or42a-/-* mutants
442 avoided the AITC tube only at the 65 minutes time point (Figure 1F), possibly by taste detection of
443 AITC via TrpA1 (we cannot exclude the possibility that volatile AITC molecules adhered to the glass
444 tube walls at this point). These findings suggest that *Or42a* plays a crucial role in mediating olfactory-
445 driven behavioral aversion to AITC. Similar percentages of genetic control and *Or42a-/-* mutants choose
446 one or the other tube at all time points (Figure Supplement 2D), indicating that *Or42a-/-* mutants are as
447 active as wild-type flies in the presence of AITC; Canton-S flies also remained similarly active in
448 presence of AITC volatiles (Figure Supplement 2C). We also confirmed that *Or42a-/-* mutants are
449 capable of odor-mediated olfactory orientation. We conducted dual-choice trap assays offering apple
450 cider vinegar vs. water as described in Matsunaga et al. (2021). Approximately 50% (median) of flies
451 released in each test ($N=8$ tests, $n=20$ females/test) were trapped and of these, 100% (median) were

452 found in the odor-baited trap (Wilcoxon-matched pairs test, $p<0.005$; Supplementary File 5). This result
453 confirms that the lack of behavioral aversion to AITC in *Or42a-/-* was not due to a generalized olfactory
454 defect in this line.

455 It has been reported that Or42a OSNs respond to a variety of fruit/fermentation volatiles,
456 including γ-hexalactone, and that some of these activators can furthermore mediate behavioral attraction
457 (Dweck et al. 2016). We thus used γ-hexalactone to test whether our behavioral assays yielded results
458 consistent with these previous findings. In consumption assays (duration=10 minutes) Canton-S flies
459 increased their feeding in the presence of volatile γ-hexalactone 1:50 vol/vol, but this effect was lost in
460 *Or42a-/-* mutants (Figure Supplement 2A). In the positional olfactory assay, a larger proportion of
461 genetic control flies than of *Or42a-/-* mutants chose either tube in presence of 1:10 vol/vol γ-
462 hexalactone at all time points (Figure Supplement 2F), suggesting that the presence of the odor increases
463 exploratory activity in control flies. Moreover, control flies showed attraction to 1:10 vol/vol γ-
464 hexalactone (at 20 and 30 minutes, one-sample signed rank tests, $p<0.05$ in both cases), but this
465 attraction was lost in *Or42a-/-* mutants (Figure Supplement 2E). Canton-S flies also showed attraction to
466 this odor (at 5, 10, and 15 minutes, $n=12$; $p<0.05$ at all those three times, Supplementary File 5).
467 Furthermore, we found that volatile γ-hexalactone does not immobilize flies (Figure Supplement 2K).
468 Thus, our behavioral assays show that volatile γ-hexalactone attracts flies and is harmless, in line with
469 previous results (Dweck et al., 2016).

470 Given that Or42a mediates both repellence to AITC and attraction to γ-hexalactone (Figure 1E-F
471 and Figure Supplement 2A and 2E-F), we next tested whether these two odorants activate additional
472 OSNs. Through exhaustive SSR from antennae and maxillary palps upon stimulation with γ-
473 hexalactone, we found that pb1a OSNs were the only OSNs activated by γ-hexalactone in basiconic,
474 intermediate, and trichoid sensilla (Figure Supplement 2L). Due to technical limitations, we were unable
475 to conduct SSR from antennal coeloconic sensilla, but Yao et al (Yao et al. 2005) reported that γ-
476 hexalactone activates OSNs in ac3b, which house Or35a OSNs (Oh et al. 2021). In contrast, AITC
477 activated several OSNs within the above mentioned sensilla types, including those in ab4a (Figure 1C).
478 Thus, we assessed whether *Or7a* and *Or35a* respectively contribute to repellence/attraction in olfactory
479 positional assays. Compared to genetic controls, *Or7a -/-* flies showed reduced aversion to AITC (Figure
480 Supplement 2G-H), while *Or35a -/-* flies lost the attraction to γ-hexalactone (Figure Supplement 2I-J).
481 These results suggest that the activation of Or42a OSNs mediates aversion to AITC in conjunction with

482 Or7a OSNs, but can also mediate attraction to γ-hexalactone if active in conjunction with Or35a OSNs.
483 Thus, our findings support a combinatorial hypothesis of odor coding with respect to these ligands and
484 indicate that the valence of Or42a-mediated behavioral responses is context-dependent (Figure
485 Supplement 2M).

486

487 **Pb1a-like OSNs in Brassicales-specialists evolved broadened sensitivity to isothiocyanates (ITCs)**

488 We next investigated how the evolutionary transitions from microbe-feeding to herbivory have
489 affected OSNs, using the reference species *Dmel* as well as species within *Scaptomyza*: the
490 microbivorous *S. hsui* (hereafter: *Shsu*) and *S. pallida* (hereafter: *Spal*), and the herbivorous Brassicales
491 specialists *Sfla* and *Smon* (Kim et al. 2021; Peláez et al. 2023). We investigated whether *Scaptomyza*
492 species have pb1-like sensilla homologous to *Dmel* pb1 and if so, the extent to which they respond to a
493 broader range of ITC compounds, since Brassicales plants release ITCs upon wounding (MacLeod et al.
494 1989; Cuellar-Nuñez et al. 2022).

495 We first validated our methods for functional characterization of sensilla in *Dmel*. We used
496 compounds that serve as diagnostic for the three sensilla types found in the maxillary palps of *Dmel* (see
497 methods for details). In addition, we used as stimuli *trans*-2-hexenal, 2-hexanol, methyl salicylate, 2-
498 heptanone and phenethyl alcohol, and Brassicales-derived isothiocyanates (ITCs) including allyl ITC
499 (AITC), isobutyl ITC (IBITC), butyl ITC (BITC), sec-butyl ITC (SBITC), and phenethyl ITC (PITC).
500 Using the diagnostic odorants, we confirmed the presence of three different types of palp sensilla (pb1,
501 pb2 and pb3) in *Dmel*. We also found that *Dmel* pb1a OSNs responded to AITC (>120 spikes/sec), but
502 not to the other ITCs tested (<10 spikes/sec, Figure 2).

503 We next characterized OSNs in pb sensilla in the four *Scaptomyza* species and used the spike
504 rate to determine if data clustered by sensilla type (Figure 2, Figure Supplement 3A). In all species,
505 sensilla fell into three functional classes akin to *Dmel* pb1, pb2 and pb3, which we termed pb1-like, pb2-
506 like, and pb3-like. The response profiles of *Scaptomyza* pb3-like OSNs were different from those of
507 *Dmel* pb3, likely because the homologs of *Or59c* and *Or85d*, which are respectively expressed in *Dmel*
508 pb3a and p3b, are unidentified in the genomes of *Scaptomyza* (Goldman-Huertas et al. 2015). We found
509 two types of pb1-like sensilla across the four *Scaptomyza* species. Both OSNs in pb1a exhibited an
510 odorant tuning pattern similar to that of *Dmel* pb1a. On the other hand, one subset of pb1b-like OSNs
511 exhibited an odorant tuning pattern akin to that of *Dmel* pb1b, while the other subset of pb1b-like OSNs

Figure 2

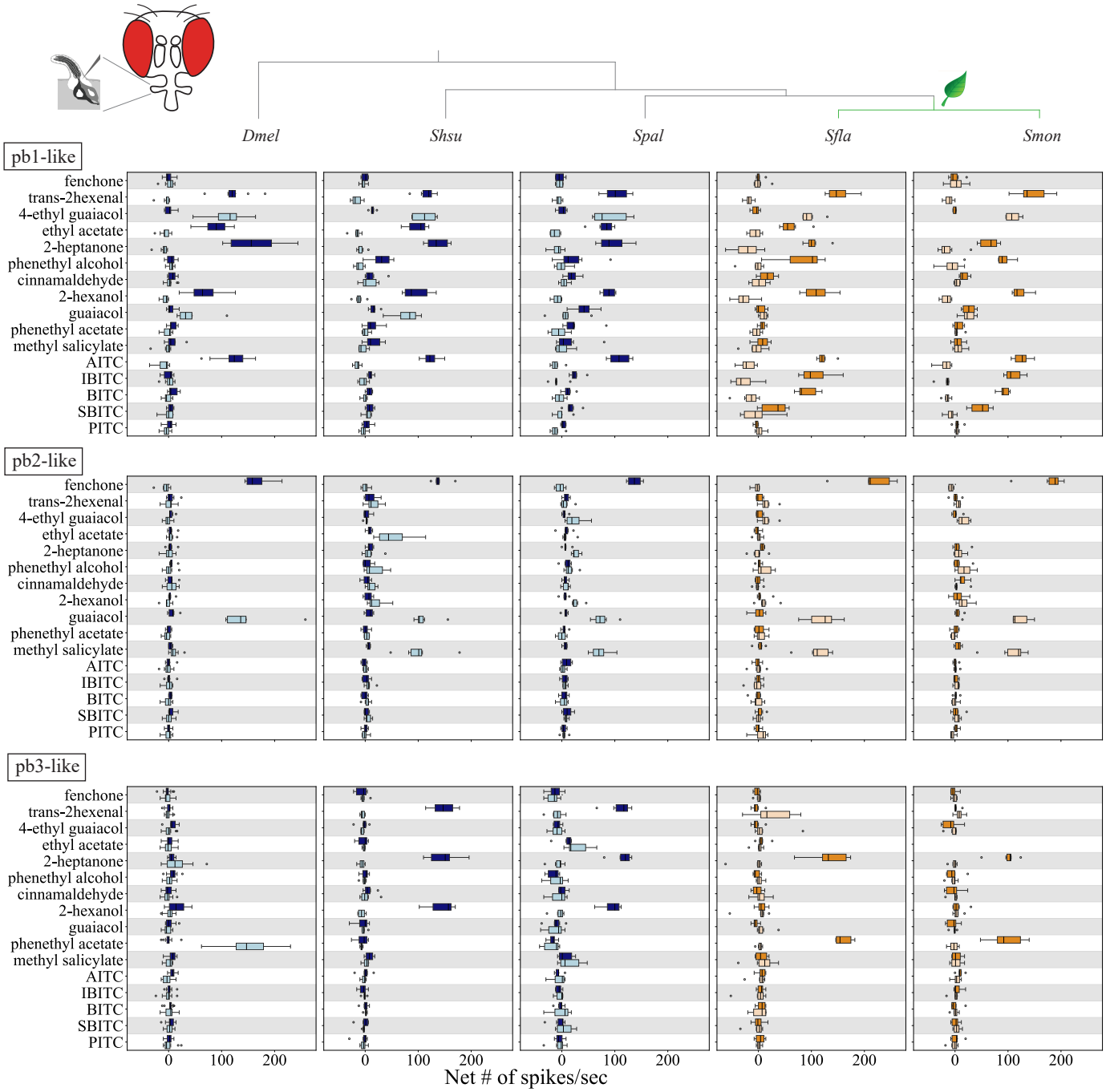
Dmel
Shsu
Spal
Sfla
Smon
pb1-like
pb2-like
pb3-like
fenchone
trans-2hexenal
4-ethyl guaiacol
ethyl acetate
2-heptanone
phenethyl alcohol
cinnamaldehyde
2-hexanol
guaiacol
phenethyl acetate
methyl salicylate
AITC
IBITC
BITC
SBITC
PITC
0
100
200
Net # of spikes/sec

consistently showed very small spike amplitudes and thus was excluded from the analysis. As in *Dmel*, AITC activated pb1a-like sensilla in all four *Scaptomyza* species (Figure 2). Notably, several other ITCs, including IBITC, BITC, and SBITC, additionally activated *Sfla* and *Smon* pb1a-like OSNs (Figure 2, first row). Methyl salicylate activated all *Scaptomyza* pb2b-like sensilla but not *Dmel* pb2b (Figure 2, second row) and interestingly, this compound is a known *Sfla* volatile attractant in natural settings (Orre et al. 2010). Furthermore, the odorant response profiles of OSNs in pb3-like sensilla were more similar between the more distantly related species *Shsu* and *Spal,* than between the more closely related species *Spal* and *Sfla,* or *Spal* and *Smon* (Figure 3, third row). For example, OSNs in pb3a-like sensilla were activated by *trans*-2-hexenal in *Shsu* and *Spal* OSNs (but not in *Sfla* or *Smon*), while *Sfla* and *Smon* OSNs (but not *Shsu* or *Spal*) were activated by phenethyl acetate (Figure Supplement 3B-C).

We also conducted SSR from pb1a (or pb1a-like) sensilla of the microbe-feeding species (*Dmel, Shsu* and *Spal*) and the Brassicales specialists (*Sfla* and *Smon*) upon stimulation with various concentrations of odorants from 10^{-5} to 10^{-2} vol/vol. For the most part, for all species and odorants, responses increased with increasing concentration (Figure Supplement 4A). For comparing odor sensitivity across species, we calculated the odorant concentration required to elicit a biological response halfway between the baseline and the maximum (50% effective concentration values, EC_{50}; Figure Supplement 4D). Interestingly, the spiking responses to γ-hexalactone stimulation were lower in *Sfla* compared to *Shsu*, and correspondingly, the EC_{50} was higher in the former (note that *Sfla* had even lower sensitivity to γ-hexalactone than *Smon*; Figure Supplement 4B Figure Supplement 4B and D). The responses of pb1a-like sensilla to *trans*-2-hexenal were higher in *Sfla* than in *Smon* (Figure Supplement 4C), and their EC_{50}s were lower in comparison to those of *Dmel* or *Shsu* (Figure Supplement 4D). Similarly, the EC_{50}s to AITC were lower in *Sfla, Smon,* and *Spal* than in *Dmel* (Figure Supplement 4D), indicating higher sensitivity to this volatile compound in those three *Scaptomyza* species. Finally, *Sfla* and *Smon* showed similar EC_{50}s to all the four ITCs tested (Figure Supplement 4D). Overall, all these findings suggest that microbe-feeding species exhibit higher γ-hexalactone sensitivity, whereas Brassicales specialists show heightened sensitivity to *trans*-2-hexenal and ITCs in general. In particular, the heightened sensitivity of *Sfla* OSNs to the general leaf odor *trans*-2-hexenal in comparison with that of *Smon* OSNs aligns with its potentially broader host range (Martin 2004; Maca 1972).

Figure 3

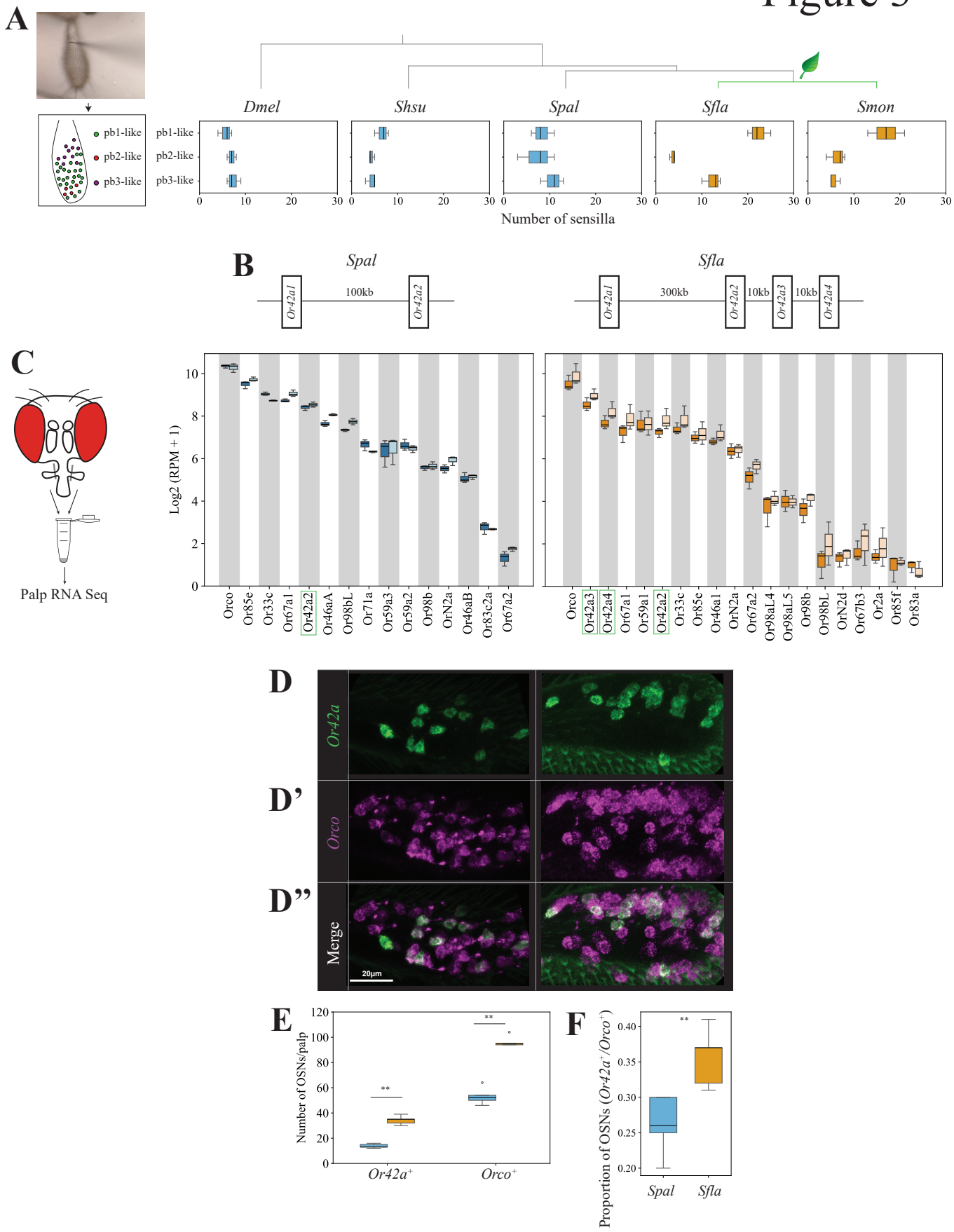
A
pb1-like
pb2-like
pb3-like
Dmel
Shsu
Spal
Sfla
Smon
Number of sensilla
B
Spal
Or42a1
100kb
Or42a2
Sfla
Or42a1
300kb
Or42a2
10kb
Or42a3
10kb
Or42a4
C
Palp RNA Seq
Log2 (RPM + 1)
Orco
Or85e
Or33c
Or67a1
Or42a2
Or46aA
Or98bL
Or71a
Or59a3
Or59a2
Or98b
OrN2a
Or46aB
Or83c2a
Or67a2
Orco
Or42a3
Or42a4
Or67a1
Or59a1
Or42a2
Or33c
Or85e
Or46a1
OrN2a
Or67a2
Or98aL4
Or98aL5
Or98b
Or98bL
OrN2d
Or67b3
Or2a
Or85f
Or83a
D
Or42a
D'
Orco
D''
Merge
20µm
E
Number of OSNs/palp
Or42a+
Orco+
F
Proportion of OSNs (Or42a+/Orco+)
Spal
Sfla

541 **Brassicales specialists have a higher number of pb1-like sensilla.**

542 We next generated anatomical maps of sensilla on the anterior part of the maxillary palps of the
543 species of *Scaptomyza* (and of *Dmel* for comparison) using diagnostic chemicals (Figure 3A, Figure
544 Supplement 5, Supplementary file 10; see methods for more detail). Interestingly, while *Dmel* had a
545 relatively randomized distribution of sensilla on the palps, consistent with previous reports (de Bruyne et
546 al. 1999), all four *Scaptomyza* species exhibited a more organized sensilla pattern, with pb1-like, pb2-
547 like, and pb3-like respectively located medially, distally, and proximally as reported in *D. mojavensis*
548 (Crowley-Gall et al. 2016).

549 The proportions of each type of palp sensilla varied within and between species (Figure 3A and
550 Figure Supplement 5). Both *Sfla* and *Smon* have a larger number of pb1-like than of pb2-like or pb3-like
551 sensilla. In contrast, *Dmel* and the other two *Scaptomyza* species had similar numbers of each sensilla
552 type. These findings suggest an expansion of pb1-like sensilla in Brassicales specialists over the course
553 of evolution. Moreover, we observed a trend in which *Sfla* and *Smon* had an overall larger number of
554 palp olfactory sensilla compared to *Dmel*, *Shsu* and *Spal* (Figure 3A, Figure Supplement 5,
555 Supplementary file 11). Within *Scaptomyza*, the larger number of sensilla in *Sfla* concurred with this
556 species' larger palp surface area (Figure Supplement 6). Taken together, these results show that
557 Brassicales plant specialists tend to have a higher proportion of pb1-like sensilla compared to microbe-
558 feeding *Drosophila* and *Scaptomyza*, suggesting that Brassicales plant specialist *Scaptomyza* species
559 may have enhanced capacity to detect volatile ITCs.

560

561 ***Sfla Or42a* is triplicated in the genome of *Sfla* and is highly expressed in the maxillary palps.**

562 We next investigated the expression of *Or* genes in maxillary palps OSNs across some of the
563 species of interest. Initially, we scanned the known genome sequences of species in the genus
564 *Scaptomyza* and found a duplication of *Or42a* in the lineage leading to all known *Scaptomyza*, while the
565 *Dmel* outgroup had a single *Or42a* homolog (Figure Supplement 7). Interestingly, within *Scaptomyza*,
566 *Sfla* exhibited serial triplicates in one of the *Or42a* duplicates, which we named *Or42a2*, *Or42a3*, and
567 *Or42a4* (Figure 3B and Figure Supplement 7), whereas *Smon* retained only two paralogs, like *Shsu* and
568 *Spal*.

569 To determine the extent of *Or* gene expression, including that of the *Or42a*s paralogs of
570 *Scaptomyza*, we conducted species- and sex-specific RNA transcriptome analyses of *Spal* and *Sfla*

571 maxillary palps (Figure 3C; Figure Supplement 8). We confirmed the expression of *Spal Or42a* and *Sfla*
572 *Or42a2-4* in these organs. Interestingly, the *Sfla Or42a* paralogs were each expressed at levels
573 comparable to those of other *Or* genes, such as *Or33c*, the homolog of which in *Dmel* is expressed in
574 OSNs of pb2a sensilla (see below). Furthermore, we confirmed the expression of homologs *Or71a*
575 (expressed in OSNs of *Dmel* pb1b), and of *Or33c/Or85e* and *Or46a* (expressed in OSNs of *Dmel* pb2a
576 and pb2b) in both *Spal* and *Sfla* maxillary palps. *Spal Or42a2* and *Sfla Or42a2-4* were expressed in the
577 OSNs of their respective palp sensilla (pb1-like), whereas *Spal Or42a1* and *Sfla Or42a1* were not.
578 *Or85d* and *Or59c* were respectively expressed in OSNs of *Dmel* pb3a and pb3b but the homologs were
579 unidentified in the genomes of *Scaptomyza* (Goldman-Huertas et al., 2015). Instead, *Or59a1, Or67a1,*
580 *Or67a2,* and *OrN2a* were strongly expressed in OSNs of both *Spal* and *Sfla,* suggesting that these
581 homologs may be expressed in pb3a or pb3b (Figure 3C). In summary, the potential conservation of *Or*
582 expression in pb1 and in pb2 sensilla, and the difference in *Or* expression in OSNs of pb3 between *Dmel*
583 and *Sfla,* may reflect the similarities and differences in their odorant response profiles (See Figure 2).
584

585 **The Brassicales specialist *Sfla* have more *Or42a*-positive-OSNs.**

586 Our transcriptome analysis revealed high expression of *Or42a* triplicates in *Sfla* maxillary palps
587 (Figure 3C), which could be due to high expression of *Or42a* in individual cells and/or a higher number
588 of *Or42a*-positive-OSNs. To distinguish between these possibilities, we quantified the number of
589 *Or42a*-positive-OSNs in the maxillary palps of *Sfla* and *Spal* using hybridization chain reaction RNA
590 fluorescent in situ hybridization (HCR RNA FISH). Due to the high sequence similarity between the
591 paralogs, we designed an RNA probe based on the conserved sequence region of *Sfla Or42a2-4* to
592 visualize all *Or42a2-4* paralog^{+} cells in *Sfla.* Similarly, we designed the *Spal Or42a2* probe to compare
593 the expression of homologs in the maxillary palps of *Sfla* and *Spal* (Figure 3B).

594 HCR RNA FISH analysis revealed that the maxillary palps of *Sfla* contained more *Or42a*-
595 positive-OSNs than those of *Spal,* as well as more *Orco*-positive-OSNs (Figure 3D-E). Because all
596 maxillary palp OSNs express Orco (Larsson et al. 2004), the number of Orco-positive OSNs represents
597 the total number of palp OSNs. The ratio of the total number of *Or42a*-positive-OSNs to the total
598 number of *Orco*-positive-OSNs was higher in *Sfla* (Figure 3F). This indicates that *Sfla* not only has
599 more *Or42a*-positive-OSNs and *Orco*-positive-OSNs, but also a greater proportion of *Or42a*-positive-
600 OSNs relative to the overall number of OSNs in the maxillary palps.

601

602 **Paralog-specific functional evolution of Or42a.**

603 We next investigated the functional evolution of *Or42a* triplicates in *Sfla*. To do this, we
604 expressed *Dmel Or42a, Spal Or42a2,* and *Sfla Or42a2-4* in *Dmel* antennal trichoid 1 (at1) OSNs in the
605 background of a null mutation for *Or67d*, the at1 cognate receptor (Kurtovic et al. 2007). We selected
606 at1 because some insects utilize host-derived chemicals as pheromones (Reddy and Guerrero 2004), and
607 certain pheromones only activate OSNs housed in trichoid sensilla in *Dmel* (Xu et al., 2005 Neuron;
608 Benton et al., 2007). We conducted SSR from at1 using six different odorant stimuli at 1:100 vol/vol.
609 We found that γ-hexalactone, *trans*-2-hexenal, and AITC strongly activated OSNs expressing *Dmel*
610 Or42a (>79 spikes/second) or *Spal* Or42a2 (>96 spikes/sec; Figure 4A-B), while IBITC, BITC and
611 SBITC evoked much weaker responses from these two paralogs (respectively <11 and 18
612 spikes/second). In contrast, OSNs expressing *Sfla* Or42a3 or *Sfla* Or42a4 were very sensitive to IBITC
613 and BITC (> 87 and 46 spikes/second, respectively), which is consistent with the response profiles of
614 *Sfla* pb1a OSNs (Figure 2). Notably, OSNs expressing *Sfla* Or42a4 showed only small responses to γ-
615 hexalactone, and *Sfla* Or42a2 was only activated by AITC (Figure 4B). These results align with the
616 niche difference between microbe-feeding flies and Brassicales specialists. Moreover, our findings
617 reveal the paralog-specific functional evolution of Or42a triplicates in *Sfla*, as different paralogs have
618 evolved distinct sensitivities to various ITC chemicals and fruit odors.

619

620 **AlphaFold2-led screening with ectopic expression of *Sfla* Or42a reveals the molecular changes**
621 **underlying changes in odor sensitivity**

622 We investigated which amino acid substitutions in *Sfla* O42a3 lead to the gain of sensitivity to
623 BITC and the decreased sensitivity to γ-hexalactone in *Sfla* Or42a4 (there are total of 32 amino acid
624 differences between *Sfla* Or42a3 and *Sfla* Or42a4, Figure Supplement 9A). For this, we predicted the 3D
625 structures of *Sfla* Or42a3 and *Sfla* Or42a4 in the cell membrane and aligned them in 3D space using
626 PyMol, and checked the overlap between Ors (Jumper et al. 2021; Mirdita et al. 2022; Benton and
627 Himmel 2023; Himmel et al. 2023).

628 We first confirmed that the predicted Local Distance Difference Test (pLDDT) scores for the
629 *Sfla* Or42a3 and *Sfla* Or42a4 structures were sufficiently high to ensure confidence in the 3D predictions

Figure 4

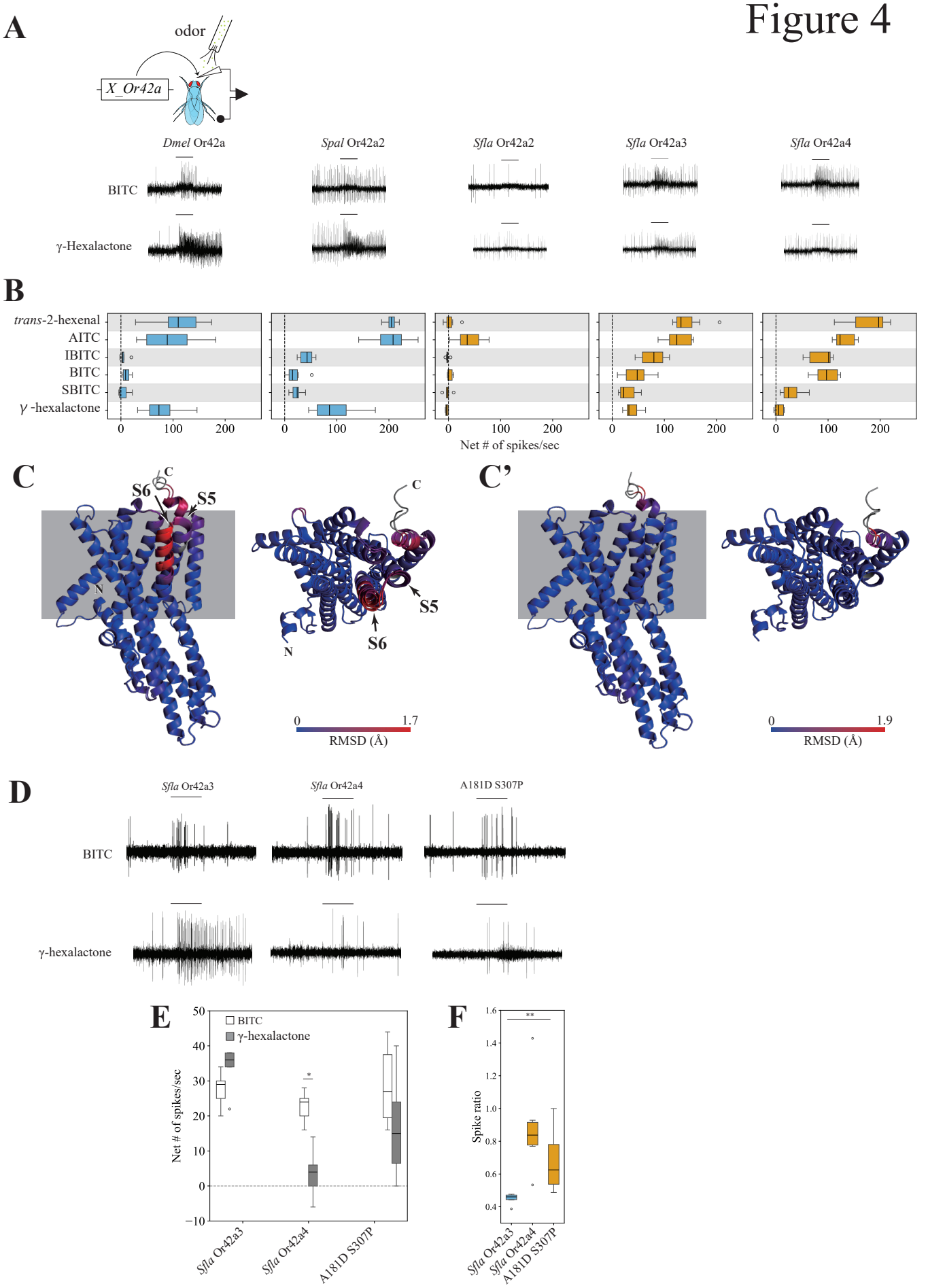
A
odor
X_Or42a
Dmel Or42a
Spal Or42a2
Sfla Or42a2
Sfla Or42a3
Sfla Or42a4
BITC
γ-Hexalactone
B
trans-2-hexenal
AITC
IBITC
BITC
SBITC
γ -hexalactone
0
100
200
Net # of spikes/sec
C
S6
S5
C
N
0
1.7
RMSD (Å)
C'
0
1.9
RMSD (Å)
D
Sfla Or42a3
Sfla Or42a4
A181D S307P
BITC
γ-hexalactone
E
BITC
γ-hexalactone
Net # of spikes/sec
50
40
30
20
10
0
−10
*
Sfla Or42a3
Sfla Or42a4
A181D S307P
F
**
Spike ratio
1.6
1.4
1.2
1.0
0.8
0.6
0.4
Sfla Or42a3
Sfla Or42a4
A181D S307P

630 in general, except for the N-terminal and C-terminal regions (Figure Supplement 9B). One of the most
631 striking differences in 3D structures between *Sfla* Or42a3 and *Sfla* Or42a4 was observed in the S5 and
632 S6 helices in the transmembrane region (~1.7Å root mean square deviation, RMSD). These helices are
633 reported to contain the ligand binding pockets (Figure 4C-C' and Figure Supplement 9B; Del Mármol et
634 al. 2021; Wang et al. 2024; Zhao et al. 2024). Importantly, we confirmed that the pLDDT scores for
635 these non-overlapping sites were above 70, indicating that the 3D predictions of these sites are reliable
636 (Figure Supplement 9B). We then substituted each of the 32 amino acids in *Sfla Or42a4* individually
637 with the corresponding residues from *Sfla* Or42a3 *in silico,* predicted the 3D structures of the chimeras,
638 and aligned them with *Sfla* Or42a4 in 3D space until the local structural differences were resolved.
639 Remarkably, the substitutions of A181D and S307P in *Sfla* Or42a3 (hereafter referred to as A181D
640 S307P) reduced the RMSD to approximately 0.1 Å in the S5 and S6 helices when aligned with *Sfla*
641 Or42a4, indicating that these two mutations effectively resolved the local structural differences (Figure
642 4C-C' and Figure Supplement 9B).

643 We then used the *Dmel* at1 empty neuron system to investigate whether these two amino acid
644 substitutions could account for the *Sfla* Or42a4 enhanced sensitivity to BITC and reduced sensitivity to
645 γ-hexalactone, in comparison with *Sfla* Or42a3. While the A181DS307P variant and the two *Sfla*
646 paralogs show similarly moderate responses to BITC (Figure 4E), the BITC to γ-hexalactone response
647 ratios of *Sfla* Or42a4 and A181D S307P were not different from each other, but were both higher than
648 that of *Sfla* Or42a3 (Figure 4F). These findings suggest that the two amino acid substitutions are
649 sufficient to increase the response to BITC relative to that of γ-hexalactone in *Sfla* Or42a4. This effect
650 was observed in flies carrying the heterozygous genotype A181D S307P/+ but not in flies with the
651 homozygous A181D S307P genotype (Compare Figure 4E-F with Figure Supplement 11), possibly due
652 to saturation effects. In summary, our findings demonstrate that the A181D and S307P substitutions are
653 critical for shifting the receptor's sensitivity from fruit odorants to ITCs.

654

655 **DISCUSSION**

656 In this study, we first discovered that plant-derived ITCs have a detrimental effect on survival of
657 *Drosophila melanogaster* (*Dmel*) through volatile exposure. We then found that these toxic electrophilic
658 volatiles are detected by Or42a, which is expressed in the maxillary palps. This Or is necessary for
659 behavioral aversion and to our knowledge, is the first known ITC-detecting olfactory detector in *Dmel*

660 and plays a role in mediating behavioral aversion to ITCs. Thus, in *Dmel*, Or42a works in combination
661 with the "wasabi" taste receptor" TrpA1 and Painless (Al-Anzi et al. 2006; Kang et al. 2010; Mandel et
662 al. 2018), and possibly with other Ors, to facilitate adaptive behavioral avoidance of these chemicals
663 through both gustatory and as we show here, olfactory chemosensory modalities.

664 We also conducted molecular evolutionary analyses, site-directed mutagenesis, and functional
665 assays to uncover the molecular mechanisms by which the Brassicales specialist *Sfla* evolved paralogous
666 copies of *Or42a* genes that responded to a broad range of electrophilic compounds emitted by their host
667 plants. Overall, our findings provide new insight into the olfactory mechanisms that allow generalist
668 insects to avoid lethal volatile toxins, and into the rapid evolution of an expanded set of more finely
669 tuned *Or*s in specialist insects that detect these volatile host-plant signals.

670 **Plant-derived volatile AITC is toxic to *Dmel* and its detection and avoidance is mediated by *Or42a*-**
671 **positive-OSNs**

672 Plants have evolved a diverse array of specialized metabolites that repel or intoxicate insects
673 (Ibanez et al. 2012). Among these, plant-derived electrophilic compounds, including *trans*-2-hexenal
674 and ITCs, are highly reactive (Noge and Becerra 2015; Tocmo et al. 2021). For example, AITC derived
675 from wasabi and other mustard and Brassicales plants causes a highly pungent sensation by activating
676 contact-mediated pain receptor TrpA1 of humans (Bell et al. 2018). Here, we found that volatile AITC
677 exerts a dose-dependent detrimental effect on *Dmel* adults (Figure 1A), underscoring the high toxicity of
678 this compound. These findings are consistent with previous findings showing that ingestion of AITC
679 decreases fly survival (Zimmermann et al. 2024) and with earlier studies on the toxic effect of volatile
680 PITC (Lichtenstein et al. 1964).

681 TrpA1 pain receptors in *Dmel* mediate the detection of ITCs and other reactive compounds by
682 taste (i.e, by contact), as they do in humans (Kim et al. 2010). In addition, the OSNs of some mustard-
683 plant specialists, such as the diamondback moth *Plutella xylostella* (via Or35a and Or49a; Liu et al.
684 2020) and *Sfla* (Matsunaga et al. 2021) also detect these compounds. However, it was unclear whether
685 non-specialists, such as *Dmel* and humans, have evolved strategies to detect these compounds via
686 olfaction. We found that Or42a and its associated OSNs are necessary for olfactory responses in *Dmel*
687 pb1a sensilla (Figure 1B-D). Furthermore, this Or was necessary for inducing olfactory aversion to
688 AITC in *Dmel* in two different behavioral contexts (Figure 1E-F and Figure Supplement 2B). It would

689 be interesting to investigate whether vertebrate also possess volatile electrophile sensors, despite the
690 different evolutionary origins from insect chemoreceptors.

691 Our results indicate that Or42a OSNs, in combination with Or7a and Or35a, contribute to
692 mediate olfactory repellence to AITC and attraction to the fruit volatile γ-hexalactone (Figure 1E-F and
693 Figure Supplement 2B-J). How does a single OSN type (*Or42a*-positive-OSNs) mediate aversion to
694 AITC while also driving attraction to γ-hexalactone? We found that AITC also activates (to a lesser
695 degree) OSNs in ab4a sensilla (Figure 1C), which expresses Or7a, a reported "generalist Or" that also
696 responds to aversive odorants (Münch and Galizia 2016). Additionally, γ-hexalactone activates Or35a-
697 expressing OSNs in the ac3B sensilla, mediating attraction to yeast odors (Yao et al., 2005; Oh et al.,
698 2021). Consistently with these results and previous reports, we found that *Or7a -/-* flies also avoided
699 AITC but less so than genetic controls (Figure Supplement 2G-H), while *Or 35a -/-* lost the attraction to
700 γ-hexalactone (Figure Supplement 2I-J). These findings suggest that the valence of the behavioral
701 responses mediated by Or42a is context dependent: Or42a mediates aversion when another aversive
702 olfactory circuit (e.g. Or7a) is active, whereas it mediates attraction when an additional attractive
703 olfactory channel is active (e.g. Or35a; Figure Supplement 2M). Future investigations at the circuit
704 level, particularly on the role of interglomerular interaction via local neurons (Haverkamp et al. 2018),
705 will be essential to further elucidate the neural mechanisms mediating these behavioral responses of
706 opposite valence.

707 **Functional evolution of *Or42a* and *Or67b* in *Scaptomyza* mustard plant specialists**

708 Insect specialization on chemically defended host plants provides a novel niche for host use if
709 they can overcome the initial toxic barrier (Ali and Agrawal, 2012). Indeed, specialized insects often use
710 these toxic compounds as olfactory "tokens" to find their host plants. Many Brassicales plants release
711 species-specific volatile ITCs (Wu et al. 2021) at particular ratios and concentrations that attract a guild
712 of specialized herbivores through olfaction. For instance, *P. xylostella* uses volatile ITCs to find suitable
713 oviposition sites (Liu et al. 2020), volatile ITCs attract *Sfla* females at least in the laboratory (Matsunaga
714 et al., 2021), and herbivorous *Scaptomyza* species have lost four *Or*s that in *Dmel* mediate attraction to
715 yeast-associated volatiles (Goldman-Huertas et al. 2015; Matsunaga et al. 2021). Interestingly, all
716 *Scaptomyza* also lost *Or7a* (which is expressed in ab4), which in *Dmel* responds to AITC (Figure 1C)
717 and participates in mediating olfactory aversion to this odor compound (Figure Supplement 2G-H).

718 Given the need for finer olfactory resolution in mustard plant specialist like *Sfla*, we investigated
719 whether the *Or*s in this lineage have undergone differentiation and specialization compared to those of
720 more generalist microbe-feeding species like *Dmel* and the close relatives of the herbivorous
721 *Scaptomyza*, which include the microbivores *Shsu* and *Spal*. We constructed functional maps of the palp
722 olfactory sensilla across all five species and found that all *Scaptomyza* species, similarly to *Dmel* (Ray et
723 al. 2008; Dweck et al. 2016), possess three distinct types of sensilla (Figure 2 and 3A, Figure
724 Supplement 3). Of particular significance is the finding that while OSNs housed in pb1a sensilla from all
725 species responded to volatile AITC, those housed in the pb1a-like sensilla of the mustard specialists *Sfla*
726 and *Smon* additionally responded to other volatile ITCs (Figure 2). Furthermore, this sensilla type was
727 expanded in these two species (Figure 3A and Figure Supplement 5).

728 Concomitantly with the functional and morphological changes described above, we found a
729 duplication of the Or (*Or42a*) housed in these ITC-responding pb1a sensilla in the lineage leading to all
730 known *Scaptomyza*, with the Brassicales-feeding *Sfla* exhibiting serial triplicates in one of the *Or42a*
731 duplicates (*Or42a2*, *Or42a3*, and *Or42a4*; Figure 3B and Figure Supplement 7). Similarly, we
732 previously reported that *Sfla* has a triplicated and positively selected Or (Or67b; Matsunaga et al. 2021)
733 which is expressed in antennal OSNs. These Ors respond to aromatic and some aliphatic ITCs in a
734 paralog-specific manner, while the *Dmel* and *Spal* Or67b single copies did not respond to any volatile
735 ITCs (Matsunaga et al. 2021). However, all three *Sfla* Or67b paralogs showed poor responses to
736 organosulfur ITCs, including AITC. In this study, on the other hand, we found that all three *Sfla* Or42a
737 paralogs responded to AITC (Figure 4B). Thus, the gene duplications and amino acid substitutions of
738 Or42a, along with those of Or67b, likely play an important role in enabling Brassicales-plant specialist
739 *Scaptomyza* species to detect a wide range of ITCs, including specific blend ratios and concentrations,
740 facilitating effective host plant location.

741 Although the pb1a sensilla of the two mustard specialist species have a broad ITC response
742 range (Figure Supplement 4A and D), *Sfla* has triplicated *Or42a*s, whereas *S. montana* (*Smon*) has only
743 one copy (Figure Supplement 7). This suggests that both the mustard plant specialization and the
744 mutations underlying the expanded ITC sensitivity range of Or42a preceded the triplication of *Or42a*.
745 What is then the adaptive value of the *Or42a* triplication? We observed that *Sfla* pb1a OSNs, which
746 express at least one of the three triplicated Or42as (Figure 3B-C), exhibited reduced sensitivity to fruit-
747 borne γ-hexalactone in comparison with *Smon* pb1a OSNs (Figure Supplement 4B). Only *Sfla* Or42a4

748 acquired the two key mutations that increased the sensitivity BITC to γ-hexalactone ratio (Figure 4E-F),
749 as evidenced by the weaker γ-hexalactone response of the chimeric Or compared to *Sfla* Or42a3 (Figure
750 4B). In agreement with these observations, structural alignment of the 3D models predicted by
751 AlphaFold2 revealed that *Smon* Or42a2 aligned well with *Sfla* Or42a3, but not with *Sfla* Or42a4 (Figure
752 Supplement 10). Based on these findings, we hypothesized the following sequence in the evolution of
753 Or42a (Figure Supplement 12): 1) mustard specialization and broadening of ITC sensitivity in the
754 ancestral drosophilid Or42a that was already sensitive to some ITCs like AITC; 2) speciation and
755 triplication of Or42a in *Sfla* but not in *Smon*; 3) relaxation of evolutionary constraints due to gene
756 duplications, allowing *Sfla* Or42a4 to reduce its sensitivity to γ-hexalactone. Thus, although mustard
757 specialization preceded the Or42a duplication, gene duplication appears to be important in driving
758 adaptation to new ecological niches.

759 Finally, what is the functional relevance of ITC-sensitive Ors expressed in various olfactory
760 organs? *Or67b* in *Sfla* is primarily expressed in the antennae (Matsunaga et al. 2021), whereas *Or42a* in
761 *Sfla* and the other drosophilids is expressed in the maxillary palps (Figure 3C). In *Dmel*, maxillary palps
762 OSNs have lower sensitivity thresholds to certain host-related compounds compared to antennal OSNs
763 (Dweck et al. 2016). Indeed, we found that the *Sfla* Or42a paralogs are much more sensitive to AITC
764 than the Or67b paralogs (Figure 4, Matsunaga et al. 2021). Odor response redundancy between antennal
765 and maxillary palp Ors could have evolved to further underpin olfactory orientation over both long and
766 short distances in drosophilids (Dweck et al. 2016). Given the proximity of Or42a OSNs to the
767 mouthparts, their activation could potentially modulate feeding behaviors, as suggested in *Dmel*
768 (Shiraiwa 2008). *Sfla* and *Smon* adult females feed on the juice that seeps into the leaf wounds they
769 create in Brassicales plants before oviposition (Peláez et al. 2022). Given this stereotyped feeding
770 behavior of adult females, while the activation of contact chemoreceptors by ITCs could help females
771 assess the suitability of an oviposition site through taste, flies may also be aided by olfactory activation
772 via the maxillary palps perhaps even before tasting the plants given their close proximity to the wounds
773 before feeding.

774 **Differential expression of *Or*s in *Scaptomyza***

775 Our maxillary palp RNA-seq expression data (Figure 3C), combined with electrophysiological
776 results showing similar patterns of odor responses in pb1-like and pb2-like sensilla OSNs (Figure 2),
777 suggest that all *Scaptomyza* species express the following *Or*s in palp sensilla OSNs: *Or42a* in pb1a-

like, *Or71a* in pb1b-like, *Or33c* and *Or85e* in pb2a-like, and *Or46a* in pb2b-like. This raises the question of which *Or*s are expressed in OSNs of pb3a- and pb3b-like sensilla in *Scaptomyza* spp. Based on our RNA-seq data, candidates included *Or67a, Or98b, Or59a,* and *OrN2a*, as they were robustly expressed in the maxillary palps (Figure 3C). Among these, only Or67a has been functionally characterized in *Dmel*, where it responds to 2-heptanone (Auer et al. 2020). Our SSR experiments showed that 2-heptanone also activated OSNs in pb3a-like (Figure 2), raising the possibility that *Scaptomyza* pb3a-like OSNs express Or67a. Alternatively, other yet uncharacterized Ors responsive to 2-heptanone might be expressed in these OSNs.

Functional evolution of ITC-responding Ors coupled with increases in OSNs

Using HCR RNA FISH, we discovered an increase in the number of *Or42a*-positive-OSNs in *Sfla* compared to *S. pallida* (*Spal*) (Figure 3D-F). Similar increases in OSNs which detect odors that bear biological significance for insects have been reported in several *Drosophila* species. For instance, the noni fruit specialist *D. sechellia* and the seasonal specialist of screw pine fruits *D. erecta* both show an increase in the number of $Or22a^{+}$ OSNs (Dekker et al. 2006; Linz et al. 2013; Auer et al. 2020). In *D. sechellia*, these OSN increases have been shown to enhance odor tracking by reducing adaptation in second-order projection neurons (Takagi et al. 2024). We hypothesize that the increase in the number of *Or42a*-positive-OSNs in *Sfla* may similarly contribute to enhance odor sensitivity and tracking during host plant finding, although this remains to be investigated.

Insight into the binding pocket of Or42a paralogs

Our results demonstrated that the Or42a paralogs from microbe-feeding species show strong responses to both AITC and γ-hexalactone (Figure 4), while the paralogs from the herbivorous *Sfla* show a notable shift in olfactory sensitivity. For example, *Sfla* Or42a3 showed moderate responses to γ-hexalactone (about an order of magnitude lower than those of the Or42a from the microbe-feeding *Spal*), and *Sfla* Or42a4 showed even less spiking activity (Figure 4D-E). Intriguingly, *Sfla* Or42a4 has a relatively higher sensitivity to BITC compared to Or42a3 (Figure 4B and D-E). These findings align with the fact that *Sfla* has undergone a full transition to herbivory. To explore the mechanisms underlying this shift from fruit-detector to ITC-detector, we employed computational and functional approaches to identify the amino acid substitutions responsible for the differences in odor sensitivities between *Sfla* Or42a3 and Or42a4.

807 The binding pocket of Ors is located within the transmembrane region, and amino acid
808 substitutions in these regions can alter the ligand's binding affinity [(Del Mármol et al. 2021; Zhao et al.
809 2024), although extracellular loops may also play an important role (Carraher et al. 2015)]. Our
810 AlphaFold2-led screening for amino acid substitutions identified two key substitutions in the
811 transmembrane portion: A181D and S307P (Figure 4C). We substituted these two amino acids and
812 found that OSNs expressing this chimeric Or have an increased BITC to γ-hexalactone response ratio
813 (Figure 4E-F). Proline is known to be a secondary structure breaker (Chou and Fasman 1978; Levitt
814 1978), and the substitution of serine by proline (S307P) likely influenced the conformation change of the
815 binding pocket, altering the protein structure, polarity, and hydrophobicity. Similarly, the substitution of
816 alanine by aspartic acid (A181D) can alter protein polarity and hydrophobicity. Thus, these two amino
817 acid changes likely account for the notable change in ligand sensitivity. However, the increased BITC to
818 γ-hexalactone spike ratio for was observed only in flies heterozygous for A181D and S307P (Or67d^{Gal4};
819 UAS-A181D S307P/+), but not in the flies homozygous for these two amino acid substitutions (compare
820 Figure 4E-F with Figure Supplement 11). Given that homozygous flies express A181D and S307P more
821 strongly than the heterozygous flies, it is possible that the OSNs' response to both BITC and γ-
822 hexalactone reached saturation in homozygous flies, obscuring further differences in spike ratios.
823 Alternatively, excessive expression of A181D and S307P may have altered the 3D structure of the
824 protein, reverting it closer to the original *Sfla* Or42a3 conformation and restoring the original binding
825 pocket. Nonetheless, the partial rescue we observed in heterologous flies indicates that A181D and
826 S307P are critical for altering the binding pocket structure, enabling the binding pocket of Ors to better
827 accommodate BITC instead of γ-hexalactone.

828

829 **CONCLUSIONS**

830 Taken together, our findings reveal that generalist insects like *D. melanogaster* have evolved
831 olfactory sensory mechanisms that allow them to detect and avoid plant-derived volatile electrophilic
832 toxins, such as ITCs. In contrast, Brassicales plant specialists like *S. flava* not only have physiological
833 adaptations to detoxify these toxic compounds but have undergone significant evolutionary sensory
834 adaptations for host recognition, including specialized ITC olfactory receptors to aid host plant location.
835 These adaptations involve the triplication of homologous Ors in the antennae (Matsunaga et al. 2021), as
836 well as in the maxillary palps (this study), which collectively expanded the sensitivity and detection

range for these and other signature hostplant odorants. Furthermore, our use of AlphaFold2, followed by site-directed mutagenesis and electrophysiology, identified critical amino acid changes for the evolution of specialized odorant receptors that we confirmed experimentally. This result also demonstrates the utility of machine learning algorithms as tools for evolutionary biology research, particularly in screening and identifying functionally relevant alleles for follow-up functional studies.

ACKNOWLEDGEMENTS

We are grateful to two anonymous reviewers, and to the editor, for their constructive comments and suggestions that improved this manuscript. T.M. thanks to Hany Dweck for valuable insights on SSR in maxillary palp sensilla, to Dr. Akinao Nose and Dr. Hiroshi Kohsaka for their advice and encouragement, and to the members of Nose' laboratory for discussions. We thank members of the Whiteman and Scott Laboratories for discussions and comments on the manuscript. The Bloomington Drosophila Stock Center, the Korean Stock Center, and the Drosophila Genomics Resource Center (NIH Grant 2P40OD010949) kindly provided fly lines. This work was supported by the Grant-in-Aid for Scientific Research Activity Start-up (T.M.), the Uehara Memorial Foundation (award number 201931028 to T.M.), the National Institute of Health (NIH) Grant (award number R35GM139653 to Gary Karpen), and the National Institute of General Medical Sciences of the NIH (award number R35GM119816 to N.K.W.).

AUTHORS' CONTRIBUTION:

All authors contributed to the experimental design, analysis, and interpretation of results. T.M. initiated the project and performed all experiments, except for the behavioral experiments (Fig. 1E-F, Figure Supplement 2A-K, and others not included in Figures), which were conducted by C.E.R; RNA FISH experiments (Fig. 3D-F), performed by B.G.H. and S.R.; and RNA-seq analysis (Fig. 3), performed by H.C.S. D.T. cloned *UAS-Or42a*s. J.W. contributed to the behavioral experiment presented in Fig. 1E. S.R.R. provided advice on SSR for T.M. T.M. wrote the manuscript in its original and revised versions with a substantial contribution from C.E.R.; C.E.R also wrote and revised the sections corresponding to the experiments she conducted. All authors, especially N.K.W. and C.E.R., provided feedback on the overall manuscript. N.K.W. supervised T.M. during the initial stages of the project.

866

867

868 **FIGURE CAPTIONS:**

869 **Figure 1: *Drosophila melanogaster* Or42a mediates volatile toxicity of allyl isothiocyanate (AITC)**
870 **and behavioral aversion to this compound**

871 **(A)** The toxic effect of various concentrations of volatile AITC to *D. melanogaster (Dmel)* flies was
872 assessed by measuring the % of mobile flies; flies were not allowed to contact the AITC source.
873 Increasing the concentration of AITC decreases the % of mobile flies, likely due to intoxication. ****
874 p<0.0001, log-rank Mantel-Cox tests against the control. **(B)** Schematic and representative trace of
875 single sensillum recording (SSR) from pb1 OSNs upon stimulation with AITC 1:100 vol/vol. The
876 horizontal bar indicates the onset of the stimulus and its duration (1 sec). **(C)** Single sensillum
877 recordings (SSR) from all *Dmel* antennae and palp basiconic sensilla upon AITC stimulation (1:100
878 vol/vol; n= 6-10 recordings/sensilla type from 6 animals). Represented here and in all the figures are the
879 control-subtracted net number of spikes/sec, unless otherwise noted. The horizontal dotted line at zero
880 indicates no response to odor stimulation. Here and thereafter, horizontal bars represent the median, the
881 edges of the boxes correspond to 25th and 75th quartiles, the whiskers denote 10th and 90th quartiles,
882 and symbols indicate outliers. **(D)** Responses from pb1 sensilla of Canton-S, w^{1118}, *Or42a-/-*, and
883 $TrpA1^{-}$ *Dmel* flies to 1:100 vol/vol AITC stimulation (n=6-10 sensilla/genotype from 3-4
884 animals/genotype). The responses of both mutant flies were compared against each other and against
885 those of w1118. Kruskal-Wallis ANOVA followed by Dunn's multiple comparisons (****p<0.001,
886 **p<0.01, *p<0.05). **(E)** Food consumption of genetic control flies (n=16) and Or42a mutants (n=14) in
887 presence or absence of a non-toxic concentration of volatile AITC (1:500 vol/vol). Both control flies and
888 mutants fed less in the presence of AITC volatiles (one-sample signed rank tests; respectively p<0.05
889 and p<0.001), but the feeding score of genetic control flies was lower than that of mutant flies (Mann-
890 Whitney U test, ***p<0.001). The dotted line at 50% indicates no feeding aversion or enhancement. **(F)**
891 Positional olfactory assay. Flies could smell, but not contact, the AITC solution (Figure Supplement
892 1C). The number of flies in the odorless and the odorous glass tubes was counted every five 5 minutes
893 until minute 35, and then again at 65 minutes. The dotted line at 50% indicates random distribution
894 between the two tubes. Genetic control flies (blue, n=15) avoided the tube closest to the odor source at
895 various time points (***p<0.005, ****p<0.001; one-sample signed rank tests against median=50%).

896 *Or42a-/-* mutants (orange, n =15) distributed randomly between the two tubes at all timepoints (p>0.05)
897 except at 65 minutes (**p<0.01).

898

899 **Figure 2: Functional characterization of maxillary palp OSNs in *Dmel* and *Scaptomyza* species.**
900 Single sensillum recordings (SSRs) from maxillary palp OSNs of *Dmel, Shsu, Spal, Sfla,* and *Smon*.
901 Stimuli (1:100 vol/vol) included diagnostic chemicals used to identify Ors in *Dmel* (see Methods), fruit
902 volatiles, green leaf volatiles (GLVs), and Brassicales plant-derived isothiocyanates (ITCs) (n=6-9 from
903 3-4 animals/species). All sensilla housed two OSNs, labeled "a" (darker color) and "b" (lighter color).
904 Their response profiles and stereotyped locations within the palp support the classification of
905 *Scaptomyza* sensilla into three types (Figure 3, Figure Supplement 5): pb1-like, pb2-like, and pb3-like.
906 While pb1a sensilla from all species responded to AITC, pb1a-like from *Sfla* and *Smon* additionally
907 responded to other ITC compounds. Mustard specialization occurred at the clade leading to the common
908 ancestor of these two species, denoted by the leaf cartoon. AITC: allyl ITC, IBITC: isobutyl ITC, BITC:
909 butyl ITC, SBITC: sec-butyl ITC, PITC: phenethyl ITC.

910

911 **Figure 3: High expression of *Or42a* paralogs and over-representation of *Or42a*-positive-OSNs in**
912 **the maxillary palp of *S. flava*.**
913 **(A)** Picture of SSR from *Sfla* maxillary palp sensilla (top left) and a representative anatomical mapping
914 of *Sfla* palp sensilla (bottom left) obtained using diagnostic chemicals. Green: pb1-like, red: pb2-like,
915 and magenta: pb3-like. Boxplots in the graph (right) represent the number of each sensilla type in *Dmel*
916 and the four *Scaptomyza* species (n=3 animals/species; see Figure Supplement 5 for individual maps).
917 Maxillary palp pb1 sensilla are over-represented in the two mustard specialists. **(B)** *Or42a* syntenic
918 regions in the genomes of *Spal* and *Sfla*, with a gene triplication in the *Sfla* genome at the syntenic
919 region of *Spal Or42a2* (*Sfla Or42a2*, *Sfla Or42a3*, and *Sfla Or42a4*). **(C)** Maxillary palp RNA seq of
920 *Spal* and *Sfla Or*s (n=3 replicates/sex and species). *Or*s with median values of the log2 (RPM +1) < 1
921 (n=3) were excluded. **(D-D")** Representative images of HCR RNA FISH from the maxillary palps of
922 *Spal* and *Sfla* showing *Or42a*-positive-OSNs (**D**, green), *Orco*-positive-OSNs (**D'**, magenta**),** and the
923 merged signals (**D'',** white indicates co-localization of *Or42a*-positive-OSNs and *Orco*-positive-OSNs).
924 Scale bar: 20µm. **(E)** Number of *Or42a*-positive-OSNs and *Orco*-positive-OSNs in one maxillary palp
925 of *Spal* (blue boxes) and *Sfla* (orange boxes, left panel) and ratio between them (right panel). Mann-
926 Whitney U tests, ** p<0.01; n=5 animals/species.

927

928 **Figure 4: Functional characterization of chimeric Or42a (A181D and S301P) and Or42a from**
929 ***Dmel*, *Spal*, and *Sfla***

930 **(A)** Representative SSR traces from *Dmel* at1 sensilla OSNs expressing species-specific *Or42a* under
931 the control of *Or67d* ^{Gal4} (fly genotype: *UAS-Or42a; Or67d* ^{Gal4}) in response to stimulation with BITC
932 and the fruit odor γ-hexalactone. **(B)** Responses of at1 OSNs (n=6-8 sensilla from 3-4 animals/genotype)
933 expressing species-specific *Or42a* upon stimulation with *trans*-2-hexenal (a general leaf odor released
934 upon leaf mechanical damage such as crushing), various ITCs produced by mustard plants (AITC,
935 IBITC, BITC, SBITC), and γ-hexalactone. **(C-C')** The 3D alignment of *Sfla* Or42a3 and *Sfla* Or42a4
936 predicted by AlphaFold2 **(C)**, and 3D alignment of *Sfla* Or42a4 and a chimeric Or42a with two amino
937 acid substitutions (A181D and S301P) in the background of *Sfla* Or42a3 **(C')**. The root mean square
938 deviation (RMSD) is visualized with a color gradient from blue (low) to red (high) in both the side (left)
939 and the top view (right). The upper and lower sections of the side view represent the extracellular and
940 the intracellular regions, respectively, with the cell membrane (gray rectangles) separating them. **(D-F)**
941 Representative SSR from *Dmel* at1 sensilla expressing heterologous *Sfla* Or42a3, Or42a4, and the
942 chimera (genotypes of *UAS-Or42a/CyO; Or67d* ^{Gal4}) upon stimulation with BITC and γ-hexalactone
943 (**D**), at1 population responses to BITC (white bars) and to γ-hexalactone (gray bars) (**E**, n=6-10 sensilla
944 from 3-4 animals/genotype; * $p<0.05$, Mann-Whitney U test), and response ratio [**F**, (response to BITC)
945 / (response to BITC + response to γ-hexalactone); ** $p<0.01$, *** $p<0.001$, Kruskal-Wallis ANOVA
946 followed by Dunn's multiple comparisons].

947

948 **FIGURE SUPPLEMENT CAPTIONS:**

949 **Figure Supplement 1: Schematic representations of behavioral assays. (A)** Mobility assay used as a
950 proxy for intoxication. Mated female flies (n=10) were placed in the upper chamber and monitored
951 every 10 minutes in presence of volatile chemicals (4 drops of a 5 µl solution in the lower chamber).
952 The top and the bottom chambers were separated by a fabric mesh, preventing direct contact between
953 the flies and the chemical solutions. **(B)** Feeding assay in presence of odors. A group of 24 hours wet-
954 starved mated female flies (n=11-15) was transferred to a vial containing a piece of filter paper
955 impregnated with 160 µl of 50 mM D-glucose dyed blue. A small container affixed to the flug vial had a
956 piece of filter paper loaded with 10 µl of an odorant solution or the solvent control, and because the
957 opening was enclosed by mesh, flies could smell but not contact the odor source. After 15 minutes, vials

958 were frozen for at least 60 minutes, the amount of blue dye in the abdomen of each fly in a vial was
959 quantified blind to treatment, and a feeding score was calculated for each vial as explained in materials
960 and methods. **(C)** Positional olfactory assay. Groups of 10-12 non-starved mated females were cold-
961 anesthetized in a small piece of clear Tygon tube, which was then used to connect the narrow ends of
962 two cut glass Pasteur pipettes. The distal end of each glass pipette was connected (via a piece of Tygon
963 tube) to a 1.75 mL glass vial containing 10 µL of the odor solution or the solvent control; a piece of
964 fabric mesh prevented insects from entering the vials containing the odor or control solutions. The
965 number of flies in each of the two tubes, as well as in the middle "release" section, were counted every
966 five minutes until minute 35, and in tests with AITC, again at 65 minutes. The % of insects that choose
967 one or the other tube over the total number of insects released, and the % of insects in the tube closest to
968 the odor source over the total number of insects that choose one or the other tube, was then calculated
969 for each time point.

970

971 **Figure Supplement 2. Behavioral data related to Figure 1D-F, and effect of γ-hexalactone in**
972 **olfactory behavior and mobility. (A)** Feeding assay, as in Figure 1E, but using γ-hexalactone (1:50
973 vol/vol). The dotted line at 50% indicates neither feeding enhancement or repellence. Canton-S flies
974 consumed more in presence than in absence of γ-hexalactone (one-sample signed rank test against
975 expected median=1, $p<0.001$, n=25), but *Or42a-/-* mutants consumed less in presence of the odor;
976 $p<0.001$, N=24). The asterisks indicate significant differences between genotypes (***$p<0.001$, Mann-
977 Whitney U test). **B-H:** Positional olfactory assays. **(B-C)** Tests with AITC 1:500 vol/vol vs mineral oil
978 (as in Figure 1F) using Canton-S flies (n=19); flies preferred the odorless tube from minute 25 onwards
979 (**B**, one sample signed rank tests, *$p<0.05$ in all cases). **(C-D)** % of flies that choose either tube in tests
980 with AITC, as a proxy for activity [calculated as: (# of flies in one or the other tube / # of flies released)
981 *100]; **C:** Canton-S flies, n=19; **D:** genetic control and *Or42a-/-* mutants, n=15 for each genotype. **(E-F)**
982 Tests using γ-hexalactone 1:10 vol/vol vs DMSO. **E:** % of genetic control and *Or42a-/-* flies in the
983 odorous tube (*$p<0.05$, one-sample signed rank tests against median=50%, n=19 for each genotype).
984 **F:** % of genetic control and *Or42a-/-* that choose either tube. Mann-Whitney U tests comparing the two
985 groups at each time point, *$p<0.05$, ***$p<0.005$. **(G-H)** Tests with *Or7a-/-* (n=15) and genetic control
986 flies (n=18) using AITC 1:500 vol/vol vs mineral oil. **G:** % of flies in the odorous tube (*$p<0.05$,
987 ***$p<0.001$, one sample signed rank tests). Differences between genotypes were significant at all time

988 points except 5 minutes (Mann-Whitney U tests). Because both genotypes were assayed in parallel,
989 control data is different from that presented in Figure 1F and panel D. **H:** % of flies that choose either
990 tube. **(I-J)** Tests with *Or35a-/-* (n=29) and genetic control flies (n=27) using γ-hexalactone 1:10 vol/vol
991 vs DMSO. **I:** % of flies in the odorous tube (*p<0.05, ***p<0.001, one sample signed rank tests).
992 Differences between genotypes were significant at all time points except 5 minutes (Mann-Whitney U
993 tests, p<0.05-0.001 in all cases). **J:** % of flies that choose either tube. Because both genotypes were
994 assayed in parallel, control data is different from that presented in panels E-F. (**K)** Mobility assay, as in
995 Figure 1A, but using γ-hexalactone at various concentrations from 1:500 to 1:2.5 vol/vol (n=). Flies
996 remained active in presence of this volatile. **(L)** SSR from all *Dmel* antennae (ab) and palp basiconic
997 (pb) sensilla to stimulation with γ-hexalactone 1:100 vol/vol. Only pb1a is activated by γ-hexalactone
998 (n= 3-6 animals/OSNs). **(M)** Activation of Or42a, in combination with distinct olfactory channels, is
999 involved in mediating both olfactory repellence to AITC (light blue arrow) and attraction to γ-
1000 hexalactone (orange arrow). Activation of Or42a in combination with Or7a or O35a likely mediates
1001 repellence and attraction, respectively.

1002

1003 **Figure Supplement 3: Hierarchical cluster analysis based on odorant response profiles across**
1004 **species. (A)** Hierarchical clusters were constructed using odorant response data from *Dmel, Shsu, Spal,*
1005 *Sfla,* and *Smon* using R studio v1.4.1717. A terminal node corresponds to a single recording from the
1006 individual sensilla; n=6-8 sensilla from 3-4 animals. **(B)** Hierarchical clusters were created for each
1007 sensilla type, including pb1-like, pb2-like, and pb3-like, using the odorant response (control-subtracted
1008 net number of spikes) average from each species as inputs. **(C)** The species phylogeny (left: Kim et al.,
1009 2021) and palp functional dendrogram (right) highlight the relevance of niche differences in shaping
1010 odorant responses. The palp functional dendrogram was generated using odorant response average for
1011 each species.

1012

1013 **Figure Supplement 4. Responses of OSNs from *Dmel* pb1a and *Scaptomyza* pb1a-like sensilla to**
1014 **stimulation with various odorant concentrations. (A)** Responses of pb1a OSNs across species upon
1015 stimulation with various concentrations (ranging from $1:10^{-2}$ to 10^{-5} vol/vol) of ethyl butyrate, γ-
1016 hexalactone, *trans*-2-hexenal, AITC, IBITC, BITC, and SBITC (n=6-8 sensilla from 3-4
1017 animals/species). The chemical structures of each compound are shown on the left. IBITC, BITC, and

1018 SBITC were only tested in *Sfla* and *Smon* pb1a, as BITC at 10^{-2} vol/vol failed to activate OSNs in pb1a
1019 from microbe-feeding species (Figure 2). **(B-C)** Responses of *Sfla* and *Smon* pb1a OSNs upon
1020 stimulation with γ-hexalactone 10^{-4} vol/vol **(B)** and *trans*-2-hexenal 10^{-4} vol/vol **(C)**. n=6-7 sensilla from
1021 3 animals/species. Mann-Whitney U tests: *p<0.05, **p<0.01. **(D)** Half maximal effective
1022 concentrations (EC_{50}) for each fly species and odorant (see Methods for calculations of EC_{50}). Kruskal-
1023 Wallis tests followed by Dunn's multiple comparisons. Different letters indicate significant differences
1024 (p-values for ethyl butyrate: *Spal* vs *Sfla* p<0.05, *Spal* vs *Smon* p<0.01; for γ-hexalactone: p<0.001; for
1025 *trans*-2-hexenal: *Dmel* vs *Smon* p<0.05, *Shsu* vs *Sfla* p <0.01, *Dmel* vs *Sfla* p<0.0001; for AITC:
1026 p<0.05). Overall, pb1a OSNs of microbe-feeding species exhibited greater sensitivity to γ-hexalactone,
1027 whereas Brassicales specialists showed higher sensitivity to *trans*-2-hexenal and AITC. *Sfla* and *Smon*
1028 showed similar sensitivities to all four ITCs tested.
1029
1030 **Figure Supplement 5: Location and percentages of the three different maxillary palp basiconic**
1031 **(pb) sensilla across species.** Classification of maxillary palp pb sensilla using SSRs and stimulation
1032 with diagnostic odorants. Data represents the proportion of pb1 and pb1-like (green), pb2 and pb2-like
1033 (red), and pb3 and pb3-like (magenta) in *Dmel, Shsu, Spal, Sfla,* and *Smon*. The schematic positions of
1034 pb sensilla in each of the three replicates (R1, R2, and R3) from each species are shown on the right.
1035 The total number of sensilla identified in each animal is indicated between parentheses.
1036
1037 **Figure Supplement 6: Maxillary palp and body area measurements across species. (A)** A
1038 representative photograph and measurement of a male *Sfla* viewed under a conventional dissection
1039 microscope. The areas of the maxillary palp and of the body are respectively indicated by the broken
1040 magenta and green lines. Body size was defined as the sum of the head, thorax (excluding legs and
1041 wings) and abdomen areas. **(B)** Data represents the palp (top) and body size (middle) areas, along with
1042 their ratio (bottom) in *Dmel, Shsu, Spal*, and *Sfla*.
1043
1044 **Figure Supplement 7: Or42a gene tree constructed by RAxML.** Maximum-likelihood gene tree with
1045 1000 bootstrap cycles using *Shsu Or42a1*, *Spal Or42a1*, *Sgra Or42a1*, *Smon Or42a1*, *Sfla Or42a1*, *Shsu*
1046 *Or42a2*, *SpalOr42a2*, *Sgra Or42a2*, *Sfla Or42a2*, *Smon Or42a*, *Sfla Or42a2*, *Sfla Or42a3*, *Sfla Or42a4*,
1047 and *Dmel Or42a* as an outgroup, generated by RAxML (v8.2.19) (Stamatakis 2014) after alignment by

1048 MAFFT v7 (Katoh and Standley 2013). Bootstrap values for the gene trees are denoted only when the
1049 values were smaller than 80. The tree was displayed by FigTree v1.4.3 (Rambaut 2009)
1050
1051 **Figure Supplement 8: Maxillary palp RNA seq of *Spal* and *Sfla Or*s.** The heatmap displays
1052 Log2[RPM+1] values of *Or*s expression in the maxillary palps of female (F) and male (M) *Sfla* and *Spal*
1053 (n=3/sex). Each column represents a replicate (e.g. *Sfla* F1: replicate #1 of female *Sfla*, *Sfla* M1:
1054 replicate #1 of male *Sfla*). Gray boxes indicate that the corresponding genes were unidentified in the
1055 genomes of the species.

1056

1057 **Figure Supplement 9: Alignment of 1D and 3D structures of amino acids of Or42a. (A)** The 1D
1058 alignment of amino acids of *Spal* Or42a2, *Sfla* Or42a3, and *Sfla* Or42a4, and *Smon* Or42a2. Red
1059 arrowheads denote the sites where site-directed-mutagenesis was performed to generate the A181D
1060 S301P chimera. **(B)** The 3D structures of *Sfla* Or42a3, *Sfla* Or42a4, A181D S301P, *Smon* Or42a2 were
1061 predicted using AlphaFold2. The colors of the amino acids indicate the predicted local distance
1062 difference test (pLDDT) scores: blue (>90), cyan (>70), yellow (> 50), and orange (<50).

1063

1064 **Figure Supplement 10: Screening of candidate amino acids by AlphaFold2 3D prediction. (A)**
1065 Lateral view of the 3D structure of A181D S301P predicted by AlphaFold2 (left). *Sfla* Or42a3-derived
1066 amino acids are indicated in magenta, and the substitutions with *Sfla* Or42a4-derived amino acids are
1067 represented in green. The middle and right panels respectively display side and top views of alignment
1068 of the predicted structures of *Sfla* Or42a3, *Sfla* Or42a4, and A181D S301P. The extracellular region at
1069 S5 and S6 (red arrows) highlights the local structural differences between *Sfla* Or42a3 and Or42a4
1070 where the A181D, S301P overlaps with the local structure of *Sfla* Or42a4. **(B)** The 3D predictions of
1071 *Sfla* Or42a3 (magenta), *Sfla* Or42a4 (green), and A181D S301P (cyan) were aligned using PyMol 2.5.3.
1072 Red rectangles highlight the sites of local structural variance between *Sfla* Or42a3 and Or42a4. The
1073 A181D S301P shows a closer alignment with Or42a4. S5' and S6' are enlarged views of S5 and S6,
1074 respectively. **(C)** The enlarged views of S5 and S6 in the alignment of 3D predictions of *Sfla* Or42a3
1075 (magenta), *Sfla* Or42a4 (green), and *Smon* Or42a2 (cyan). **(D)** The 3D alignment of *Sfla* Or42a3 and
1076 *Smon* Or42a2 predicted by AlphaFold2. The root mean square deviation (RMSD) is visualized with a
1077 color gradient.

1078

1079 **Figure Supplement 11: Responses of OSNs expressing homozygous Or42a to stimulation with**
1080 **BITC and γ-hexalactone.** Left: responses of OSNs expressing homozygous *Sfla* Or42a3, *Sfla* Or42a4,
1081 or A181D S307P (*UAS-Or42a; Or67d* ^{Gal4}) to stimulation with BITC (white) and γ-hexalactone (grey)
1082 (n=16-30 from 5-10 animals). Right: ratio between responses to BITC and the sum of the responses
1083 evoked by stimulation with BITC and γ-hexalactone. Kruskal-Wallis followed by Dunn's multiple
1084 comparisons, *$p<0.05$.

1085

1086 **Figure Supplement 12: A model for the evolution of Or42a in *Sfla, Smon* and *Spal*.** The evolution of
1087 Or42a begins with a shift in the ligand specificity of an ancestral Or42a (a), which was tuned to fruit-
1088 borne odors such as γ-hexalactone and limited ITCs (i.e. AITC), and later broadened to detect a wider
1089 range of ITCs (b). Subsequent gene triplication of *Sfla Or42a* resulted in three paralogous genes (c: *Sfla*
1090 *Or42a2, Sfla Or42a3,* and *Sfla Or42a4*). The lineage leading to *Sfla* Or42a2 and *Sfla* Or42a4
1091 experienced a reduction in sensitivity to γ-hexalactone, while both *Sfla* Or42a3 and *Smon* Or42a2
1092 retained sensitivity to γ-hexalactone.

1093

1094 **SUPPLEMENTARY MATERIAL AND METHODS:**

1095 **Measurement of maxillary palps and body size**
1096 Two-to-ten-days old male *Dmel, Shsu, Spal,* and *Sfla* flies with their heads facing up and their bodies
1097 sideway were mounted and imaged using a commercial camera under a conventional microscope. The
1098 areas of the maxillary palps and the body (head, thorax excluding legs and wings, and abdomen) were
1099 measured using ImageJ v1.54.

1100 **Dilution series**
1101 *Trans*-2-hexenal, AITC, IBITC, SBITC, and ethyl butyrate were diluted in mineral oil, and γ-
1102 hexalactone was diluted in DMSO to 10^{-5} to 10^{-2} vol/vol. Half maximal effective concentration (EC50)
1103 was generated by GraphPad Prism v10.2.1.

1104 **Construction of Or42a gene tree**

1105 The amino acid sequences of *Dmel Or42a,* and *Sfla Or42a1, Sfla Or42a2, Sfla Or42a3,* and *Sfla Or42a4*
1106 were obtained from Flybase (2024_01), and Goldman-Huertas et al., 2015. Blast searches were
1107 conducted to annotate *Shsu Or42a1, Spal Or42a1, Sgra Or42a1, Smon Or42a1, Sfla Or42a1, Shsu*
1108 *Or42a2, Spal Or42a2, Sgra Or42a2,* and *Smon Or42a2*, using *Sfla Or42a1* and *Sfla Or42a2* as query
1109 against the genomes of *Shsu* (ASM1815282v1), *Spal* (ASM1815296v1), *S. graminum*
1110 (ASM1890183v1), and *Smon* (ASM1890430v1). Amino acid sequences of *Shsu Or42a1, Spal Or42a1,*
1111 *Sgra Or42a1, Smon Or42a1, Sfla Or42a1, Shsu Or42a2, SpalOr4* (Katoh and Standley 2013)*2a2, Sgra*
1112 *Or42a2, Sfla Or42a2, Smon Or42a, Sfla Or42a2, Sfla Or42a3, Sfla Or42a4,* and *Dmel Or42a* were
1113 aligned by MAFFT v7.511 with JTT as scoring matrix for amino acid sequences with L-INS-i strategy.
1114 Maximum-likelihood gene tree with 1000 bootstrap cycles using the above sequences were constructed
1115 with RAxML (v8.2.19)(Stamatakis 2014). GAMMA model of rate heterogeneity was applied. CDS and
1116 alignment of *Or42a* are included in Supplementary files 12 and 13, respectively.

1117 **SUPPLEMENTARY FILES:**

1118 Supplementary file 1: Chemical list

1119 Supplementary file 2: Control-subtracted net number of spikes/sec and EC_{50} obtained from SSRs

1120 Supplementary file 3: Immobility assay data

1121 Supplementary file 4: Consumption assay data

1122 Supplementary file 5: Olfactory positional assay data and trap assay

1123 Supplementary file 6: Expression intensity from maxillary palp RNA-seq

1124 Supplementary file 7: OSNs counts from RNA FISH

1125 Supplementary file 8: Primer list

1126 Supplementary file 9: AlphaFold2 (Colabfold) prediction in pdb format

1127 Supplementary file 10: Pb sensilla counts from SSR experiments

1128 Supplementary file 11: Measurements (area) of maxillary palp and body

1129 Supplementary file 12: CDS of *Or42a* homologs in fasta format

1130 Supplementary file 13: Alignment of *Or42a* homologs in fasta format

1131

1132 **DATA AVAILABILITY:**

1133 The data presented in this study are available on request from the corresponding author.

1134

1135 **REFERENCES**

1136 Aguilar JM, Gloss AD, Suzuki HC, Verster KI, Singhal M, Hoff J, Grebenok R, Nabity PD, Behmer ST,
1137 Whiteman NK. 2024. Insights into the evolution of herbivory from a leaf‐mining fly.
1138 *Ecosphere* [Internet] 15. Available from:
1139 https://esajournals.onlinelibrary.wiley.com/doi/10.1002/ecs2.4764

1140 Ahuja I, Rohloff J, Bones AM. 2010. Defence mechanisms of Brassicaceae: implications for plant-insect
1141 interactions and potential for integrated pest management. A review. *Agron. Sustain. Dev.*
1142 30:311–348.

1143 Al-Anzi B, Tracey WD Jr, Benzer S. 2006. Response of Drosophila to wasabi is mediated by painless,
1144 the fly homolog of mammalian TRPA1/ANKTM1. *Curr. Biol.* 16:1034–1040.

1145 Anders S, Pyl PT, Huber W. 2015. HTSeq--a Python framework to work with high-throughput
1146 sequencing data. *Bioinformatics* 31:166–169.

1147 Auer TO, Khallaf MA, Silbering AF, Zappia G, Ellis K, Álvarez-Ocaña R, Arguello JR, Hansson BS,
1148 Jefferis GSXE, Caron SJC, et al. 2020. Olfactory receptor and circuit evolution promote host
1149 specialization. *Nature* 579:402–408.

1150 Becher PG, Bengtsson M, Hansson BS, Witzgall P. 2010. Flying the fly: long-range flight behavior of
1151 Drosophila melanogaster to attractive odors. *J. Chem. Ecol.* 36:599–607.

1152 Bell L, Oloyede OO, Lignou S, Wagstaff C, Methven L. 2018. Taste and flavor perceptions of
1153 glucosinolates, isothiocyanates, and related compounds. *Mol. Nutr. Food Res.* 62:e1700990.

1154 Benton R, Himmel NJ. 2023. Structural screens identify candidate human homologs of insect
1155 chemoreceptors and cryptic Drosophila gustatory receptor-like proteins. *Elife* 12:e85537.

1156 Bernays E, Chapman R. 1987. The evolution of deterrent responses in plant-feeding insects. In:
1157 Proceedings in Life Sciences. New York, NY: Springer New York. p. 159–173.

1158 Bischof J, Maeda RK, Hediger M, Karch F, Basler K. 2007. An optimized transgenesis system for
1159 Drosophila using germ-line-specific phiC31 integrases. *Proc. Natl. Acad. Sci. U. S. A.* 104:3312–
1160 3317.

1161 de Bruyne M, Clyne PJ, Carlson JR. 1999. Odor coding in a model olfactory organ: the Drosophila
1162 maxillary palp. *J. Neurosci.* 19:4520–4532.

1163 Butterwick JA, Del Mármol J, Kim KH, Kahlson MA, Rogow JA, Walz T, Ruta V. 2018. Cryo-EM
1164 structure of the insect olfactory receptor Orco. *Nature* 560:447–452.

1165 Carraher C, Dalziel J, Jordan MD, Christie DL, Newcomb RD, Kralicek AV. 2015. Towards an
1166 understanding of the structural basis for insect olfaction by odorant receptors. *Insect Biochem.*
1167 *Mol. Biol.* 66:31–41.

1168 Chen S, Zhou Y, Chen Y, Gu J. 2018. fastp: an ultra-fast all-in-one FASTQ preprocessor.
1169 *Bioinformatics* 34:i884–i890.

1170 Chen Y-CD, Dahanukar A. 2020. Recent advances in the genetic basis of taste detection in Drosophila.
1171 *Cell. Mol. Life Sci.* 77:1087–1101.

1172 Chou PY, Fasman GD. 1978. Prediction of the secondary structure of proteins from their amino acid
1173 sequence. *Adv. Enzymol. Relat. Areas Mol. Biol.* 47:45–148.

1174 Couto A, Alenius M, Dickson BJ. 2005. Molecular, anatomical, and functional organization of the
1175 Drosophila olfactory system. *Curr. Biol.* 15:1535–1547.

1176 Crowley-Gall A, Date P, Han C, Rhodes N, Andolfatto P, Layne JE, Rollmann SM. 2016. Population
1177 differences in olfaction accompany host shift in Drosophila mojavensis. *Proc. Biol. Sci.*
1178 [Internet] 283. Available from: https://www.ncbi.nlm.nih.gov/pmc/articles/PMC5013806/

1179 Cuellar-Nuñez ML, Luzardo-Ocampo I, Lee-Martínez S, Larrauri-Rodríguez M, Zaldívar-Lelo de
1180 Larrea G, Pérez-Serrano RM, Camacho-Calderón N. 2022. Isothiocyanate-Rich Extracts from
1181 Cauliflower (Brassica oleracea Var. Botrytis) and Radish (Raphanus sativus) Inhibited Metabolic
1182 Activity and Induced ROS in Selected Human HCT116 and HT-29 Colorectal Cancer Cells. *Int.*
1183 *J. Environ. Res. Public Health* [Internet] 19. Available from:
1184 http://dx.doi.org/10.3390/ijerph192214919

1185 Dekker T, Ibba I, Siju KP, Stensmyr MC, Hansson BS. 2006. Olfactory shifts parallel superspecialism
1186 for toxic fruit in Drosophila melanogaster sibling, D. sechellia. *Curr. Biol.* 16:101–109.

1187 Del Mármol J, Yedlin MA, Ruta V. 2021. The structural basis of odorant recognition in insect olfactory
1188 receptors. *Nature* 597:126–131.

1189 Dobin A, Davis CA, Schlesinger F, Drenkow J, Zaleski C, Jha S, Batut P, Chaisson M, Gingeras TR.
1190 2013. STAR: ultrafast universal RNA-seq aligner. *Bioinformatics* 29:15–21.

1191 Dobler S, Dalla S, Wagschal V, Agrawal AA. 2012. Community-wide convergent evolution in insect
1192 adaptation to toxic cardenolides by substitutions in the Na,K-ATPase. *Proc. Natl. Acad. Sci. U.*
1193 *S. A.* 109:13040–13045.

1194 Dweck HK, Ebrahim SA, Khallaf MA, Koenig C, Farhan A, Stieber R, Weißflog J, Svatoš A, Grosse-
1195 Wilde E, Knaden M, et al. 2016. Olfactory channels associated with the Drosophila maxillary

1196 palp mediate short- and long-range attraction. *Elife* [Internet] 5. Available from:
1197 https://www.ncbi.nlm.nih.gov/pmc/articles/PMC4927298/

1198 Dweck HKM, Carlson JR. 2020. Molecular logic and evolution of bitter taste in Drosophila. *Curr. Biol.*
1199 30:17-30.e3.

1200 Gloss A, Nelson Dittrich AC, Lapoint R, Goldman-Huertas B, Verster KI, Pelaez JL, Nelson AD,
1201 Aguilar JM, Armstrong E, Charboneau JLM, et al. 2019. Evolution of herbivory remodels a
1202 Drosophila genome. *bioRxiv* [Internet]. Available from:
1203 https://www.biorxiv.org/content/10.1101/767160v1

1204 Gloss AD, Brachi B, Feldmann MJ, Groen SC, Bartoli C, Gouzy J, LaPlante ER, Meyer CG, Pyon HS,
1205 Rogan SC, et al. 2017. Genetic variants affecting plant size and chemical defenses jointly shape
1206 herbivory in*Arabidopsis*. *bioRxiv* [Internet]:156299. Available from:
1207 https://www.biorxiv.org/content/10.1101/156299v1

1208 Gloss AD, Vassão DG, Hailey AL, Nelson Dittrich AC, Schramm K, Reichelt M, Rast TJ, Weichsel A,
1209 Cravens MG, Gershenzon J, et al. 2014. Evolution in an ancient detoxification pathway is
1210 coupled with a transition to herbivory in the drosophilidae. *Mol. Biol. Evol.* 31:2441–2456.

1211 Goldman-Huertas B, Mitchell RF, Lapoint RT, Faucher CP, Hildebrand JG, Whiteman NK. 2015.
1212 Evolution of herbivory in Drosophilidae linked to loss of behaviors, antennal responses, odorant
1213 receptors, and ancestral diet. *Proceedings of the National Academy of Sciences* 112:3026–3031.

1214 Gonzalez F, Witzgall P, Walker WB. 2016. Protocol for heterologous expression of insect odourant
1215 receptors in Drosophila. *Front. Ecol. Evol.* [Internet] 4. Available from:
1216 https://www.frontiersin.org/journals/ecology-and-
1217 evolution/articles/10.3389/fevo.2016.00024/full

1218 Hashimoto Y, Yoshimura M, Huang R-N. 2019. Wasabi versus red imported fire ants: preliminary test
1219 of repellency of microencapsulated allyl isothiocyanate against Solenopsis invicta
1220 (Hymenoptera: Formicidae) using bait traps in Taiwan. *Appl. Entomol. Zool. (Jpn.)* 54:193–196.

1221 Haverkamp A, Hansson BS, Knaden M. 2018. Combinatorial codes and labeled lines: How insects use
1222 olfactory cues to find and judge food, mates, and oviposition sites in complex environments.
1223 *Front. Physiol.* 9:49.

1224 Himmel NJ, Moi D, Benton R. 2023. Remote homolog detection places insect chemoreceptors in a
1225 cryptic protein superfamily spanning the tree of life. *Curr. Biol.* 33:5023-5033.e4.

1226 Hopkins RJ, van Dam NM, van Loon JJA. 2009. Role of glucosinolates in insect-plant relationships and
1227 multitrophic interactions. *Annu. Rev. Entomol.* 54:57–83.

1228 Humphrey PT, Gloss AD, Alexandre NM, Villalobos MM, Fremgen MR, Groen SC, Meihls LN, Jander
1229 G, Whiteman NK. 2016. Aversion and attraction to harmful plant secondary compounds jointly
1230 shape the foraging ecology of a specialist herbivore. *Ecol. Evol.* 6:3256–3268.

1231 Ibanez S, Gallet C, Després L. 2012. Plant insecticidal toxins in ecological networks. *Toxins (Basel)*
1232 4:228–243.

1233 Iorio R, Celenza G, Petricca S. 2022. Multi-target effects of ß-caryophyllene and carnosic acid at the
1234 Crossroads of mitochondrial dysfunction and neurodegeneration: From oxidative stress to
1235 microglia-mediated neuroinflammation. *Antioxidants (Basel)* 11:1199.

1236 Jumper J, Evans R, Pritzel A, Green T, Figurnov M, Ronneberger O, Tunyasuvunakool K, Bates R,
1237 Žídek A, Potapenko A, et al. 2021. Highly accurate protein structure prediction with AlphaFold.
1238 *Nature* 596:583–589.

1239 Kang K, Pulver SR, Panzano VC, Chang EC, Griffith LC, Theobald DL, Garrity PA. 2010. Analysis of
1240 Drosophila TRPA1 reveals an ancient origin for human chemical nociception. *Nature* 464:597–
1241 600.

1242 Katoh K, Standley DM. 2013. MAFFT multiple sequence alignment software version 7: improvements
1243 in performance and usability. *Mol. Biol. Evol.* 30:772–780.

1244 Kim BY, Wang JR, Miller DE, Barmina O, Delaney E, Thompson A, Comeault AA, Peede D,
1245 D'Agostino ERR, Pelaez J, et al. 2021. Highly contiguous assemblies of 101 drosophilid
1246 genomes. *Elife* [Internet] 10. Available from: https://pubmed.ncbi.nlm.nih.gov/34279216/

1247 Kim SH, Lee Y, Akitake B, Woodward OM, Guggino WB, Montell C. 2010. *Drosophila* TRPA1
1248 channel mediates chemical avoidance in gustatory receptor neurons. *Proceedings of the National*
1249 *Academy of Sciences* 107:8440–8445.

1250 Kurtovic A, Widmer A, Dickson BJ. 2007. A single class of olfactory neurons mediates behavioural
1251 responses to a Drosophila sex pheromone. *Nature* 446:542–546.

1252 Larsson MC, Domingos AI, Jones WD, Chiappe ME, Amrein H, Vosshall LB. 2004. Or83b encodes a
1253 broadly expressed odorant receptor essential for Drosophila olfaction. *Neuron* 43:703–714.

1254 Levitt M. 1978. Conformational preferences of amino acids in globular proteins. *Biochemistry* 17:4277–
1255 4285.

1256 Lichtenstein EP, Morgan DG, Mueller CH. 1964. Insecticides in Nature, Naturally Occurring
1257 Insecticides in Cruciferous Crops. *J. Agric. Food Chem.* 12:158–161.

1258 Linz J, Baschwitz A, Strutz A, Dweck HKM, Sachse S, Hansson BS, Stensmyr MC. 2013. Host plant-
1259 driven sensory specialization in Drosophila erecta. *Proc. Biol. Sci.* 280:20130626.

1260 Liu X-L, Zhang J, Yan Q, Miao C-L, Han W-K, Hou W, Yang K, Hansson BS, Peng Y-C, Guo J-M, et
1261 al. 2020. The molecular basis of host selection in a Crucifer-specialized moth. *Curr. Biol.*
1262 30:4476-4482.e5.

1263 MacLeod AJ, MacLeod G, Reader G. 1989. Evidence for the occurrence of butyl- and
1264 isobutylglucosinolates in seeds of Brassica oleracea. *Phytochemistry* 28:1405–1407.

1265 Mandel SJ, Shoaf ML, Braco JT, Silver WL, Johnson EC. 2018. Behavioral aversion to AITC requires
1266 both painless and dTRPA1 in Drosophila. *Front. Neural Circuits* 12:45.

1267 Mantel N. 1966. Evaluation of survival data and two new rank order statistics arising in its
1268 consideration. *Cancer Chemother. Rep.* 50:163–170.

1269 Mariani V, Biasini M, Barbato A, Schwede T. 2013. lDDT: a local superposition-free score for
1270 comparing protein structures and models using distance difference tests. *Bioinformatics*
1271 29:2722–2728.

1272 Martin NA. 2004. History of an invader,Scaptomyza flava(fallen, 1823) (Diptera: Drosophilidae). *N. Z.*
1273 *J. Zool.* 31:27–32.

1274 Matsunaga T, Reisenman CE, Goldman-Huertas B, Brand P, Miao K, Suzuki HC, Verster KI, Ramírez
1275 SR, Whiteman NK. 2021. Evolution of Olfactory Receptors Tuned to Mustard Oils in
1276 Herbivorous Drosophilidae. *Mol. Biol. Evol.* 39:msab362.

1277 Mirdita M, Schütze K, Moriwaki Y, Heo L, Ovchinnikov S, Steinegger M. 2022. ColabFold: making
1278 protein folding accessible to all. *Nat. Methods* 19:679–682.

1279 Mithöfer A, Boland W. 2012. Plant defense against herbivores: chemical aspects. *Annu. Rev. Plant Biol.*
1280 63:431–450.

1281 Münch D, Galizia CG. 2016. DoOR 2.0--Comprehensive Mapping of Drosophila melanogaster Odorant
1282 Responses. *Sci. Rep.* 6:21841.

1283 Noge K, Becerra JX. 2015. 4-Oxo-(E)-2-hexenal produced by Heteroptera induces permanent
1284 locomotive impairment in crickets that correlates with free thiol depletion. *FEBS Open Bio*
1285 5:319–324.

1286 Oh SM, Jeong K, Seo JT, Moon SJ. 2021. Multisensory interactions regulate feeding behavior in
1287 Drosophila. *Proc. Natl. Acad. Sci. U. S. A.* 118:e2004523118.

1288 Orre GUS, Wratten SD, Jonsson M, Hale RJ. 2010. Effects of an herbivore-induced plant volatile on
1289 arthropods from three trophic levels in brassicas. *Biol. Control* 53:62–67.

1290 Peláez JN, Gloss AD, Goldman-Huertas B, Kim B, Lapoint RT, Pimentel-Solorio G, Verster KI, Aguilar
1291 JM, Nelson Dittrich AC, Singhal M, et al. 2023. Evolution of chemosensory and detoxification
1292 gene families across herbivorous Drosophilidae. *G3* [Internet] 13. Available from:
1293 http://dx.doi.org/10.1093/g3journal/jkad133

1294 Peláez JN, Gloss AD, Ray JF, Chaturvedi S, Haji D, Charboneau JLM, Verster KI, Whiteman NK.
1295 2022. Evolution and genomic basis of the plant-penetrating ovipositor: a key morphological trait
1296 in herbivorous Drosophilidae. *Proc. Biol. Sci.* 289:20221938.

1297 Rambaut A. 2009. FigTree, version 1.4.3. *Computer program distributed by the author, website:*
1298 *http://tree.bio.ed.ac.uk/software/figtree/[accessed January 4, 2011]* [Internet]. Available from:

1299 https://scholar.google.com/citations?view_op=view_citation&hl=en&citation_for_view=JiYPDf
1300 oAAAAJ:W5xh706n7nkC

1301 Ray A, van der Goes van Naters W, Carlson JR. 2008. A regulatory code for neuron-specific odor
1302 receptor expression. *PLoS Biol.* 6:e125.

1303 Ray A, van Naters W van der G, Shiraiwa T, Carlson JR. 2007. Mechanisms of odor receptor gene
1304 choice in Drosophila. *Neuron* 53:353–369.

1305 Reichstein T, von Euw J, Parsons JA, Rothschild M. 1968. Heart poisons in the monarch butterfly. Some
1306 aposematic butterflies obtain protection from cardenolides present in their food plants. *Science*
1307 161:861–866.

1308 Reisenman CE, Scott K. 2019. Food-derived volatiles enhance consumption in Drosophila
1309 melanogaster. *J. Exp. Biol.* 222:jeb202762.

1310 Scott K. 2018. Gustatory processing in Drosophila melanogaster. *Annu. Rev. Entomol.* 63:15–30.

1311 Semmelhack JL, Wang JW. 2009. Select Drosophila glomeruli mediate innate olfactory attraction and
1312 aversion. *Nature* 459:218–223.

1313 Shiraiwa T. 2008. Multimodal chemosensory integration through the maxillary palp in Drosophila. *PLoS*
1314 *One* 3:e2191.

1315 Southwood T. 1972. insect/plant relationship--an evolutionary perspective. Available from:
1316 https://www.semanticscholar.org/paper/insect%2Fplant-relationship--an-evolutionary-
1317 Southwood/635ed400c02b62dca75e90d7ee3e664383d480be

1318 Stamatakis A. 2014. RAxML version 8: a tool for phylogenetic analysis and post-analysis of large
1319 phylogenies. *Bioinformatics* 30:1312–1313.

1320 Stensmyr MC, Dweck HKM, Farhan A, Ibba I, Strutz A, Mukunda L, Linz J, Grabe V, Steck K,
1321 Lavista-Llanos S, et al. 2012. A conserved dedicated olfactory circuit for detecting harmful
1322 microbes in Drosophila. *Cell* 151:1345–1357.

1323 Takagi S, Sancer G, Abuin L, Stupski SD, Roman Arguello J, Prieto-Godino LL, Stern DL, Cruchet S,
1324 Álvarez-Ocaña R, Wienecke CFR, et al. 2024. Olfactory sensory neuron population expansions
1325 influence projection neuron adaptation and enhance odour tracking. *Nat. Commun.* 15:7041.

1326 Tocmo R, Veenstra JP, Huang Y, Johnson JJ. 2021. Covalent modification of proteins by plant-derived
1327 natural products: Proteomic approaches and biological impacts. *Proteomics* 21:e1900386.

1328 Wang Y, Qiu L, Wang Bing, Guan Z, Dong Z, Zhang J, Cao S, Yang L, Wang Bo, Gong Z, et al. 2024.
1329 Structural basis for odorant recognition of the insect odorant receptor OR-Orco heterocomplex.
1330 *Science* 384:1453–1460.

1331 War AR, Paulraj MG, Ahmad T, Buhroo AA, Hussain B, Ignacimuthu S, Sharma HC. 2012.
1332 Mechanisms of plant defense against insect herbivores. *Plant Signal. Behav.* 7:1306–1320.

1333 Whiteman NK, Gloss AD, Sackton TB, Groen SC, Humphrey PT, Lapoint RT, Sønderby IE, Halkier
1334 BA, Kocks C, Ausubel FM, et al. 2012. Genes involved in the evolution of herbivory by a leaf-
1335 mining, Drosophilid fly. *Genome Biol. Evol.* 4:900–916.

1336 Whiteman NK, Groen SC, Chevasco D, Bear A, Beckwith N, Gregory TR, Denoux C, Mammarella N,
1337 Ausubel FM, Pierce NE. 2011. Mining the plant-herbivore interface with a leafmining
1338 Drosophila of Arabidopsis. *Mol. Ecol.* 20:995–1014.

1339 Winde I, Wittstock U. 2011. Insect herbivore counteradaptations to the plant glucosinolate-myrosinase
1340 system. *Phytochemistry* 72:1566–1575.

1341 Wu X, Huang H, Childs H, Wu Y, Yu L, Pehrsson PR. 2021. Glucosinolates in Brassica vegetables:
1342 Characterization and factors that influence distribution, content, and intake. *Annu. Rev. Food Sci.*
1343 *Technol.* 12:485–511.

1344 Yaffe PB, Power Coombs MR, Doucette CD, Walsh M, Hoskin DW. 2015. Piperine, an alkaloid from
1345 black pepper, inhibits growth of human colon cancer cells via G1 arrest and apoptosis triggered
1346 by endoplasmic reticulum stress: PIPERINE INHIBITS COLON CANCER CELL GROWTH.
1347 *Mol. Carcinog.* 54:1070–1085.

1348 Yao CA, Ignell R, Carlson JR. 2005. Chemosensory coding by neurons in the coeloconic sensilla of the
1349 Drosophila antenna. *J. Neurosci.* 25:8359–8367.

1350 Zhao J, Chen AQ, Ryu J, Del Mármol J. 2024. Structural basis of odor sensing by insect heteromeric
1351 odorant receptors. *Science* 384:1460–1467.

1352 Zimmermann C, Dähn S, Wagner AE. 2024. Effect of allyl-isothiocyanate on survival and antimicrobial
1353 peptide expression following oral bacterial infections in Drosophila melanogaster. *Front.*
1354 *Immunol.* 15:1404086.

Supp. Figure 1

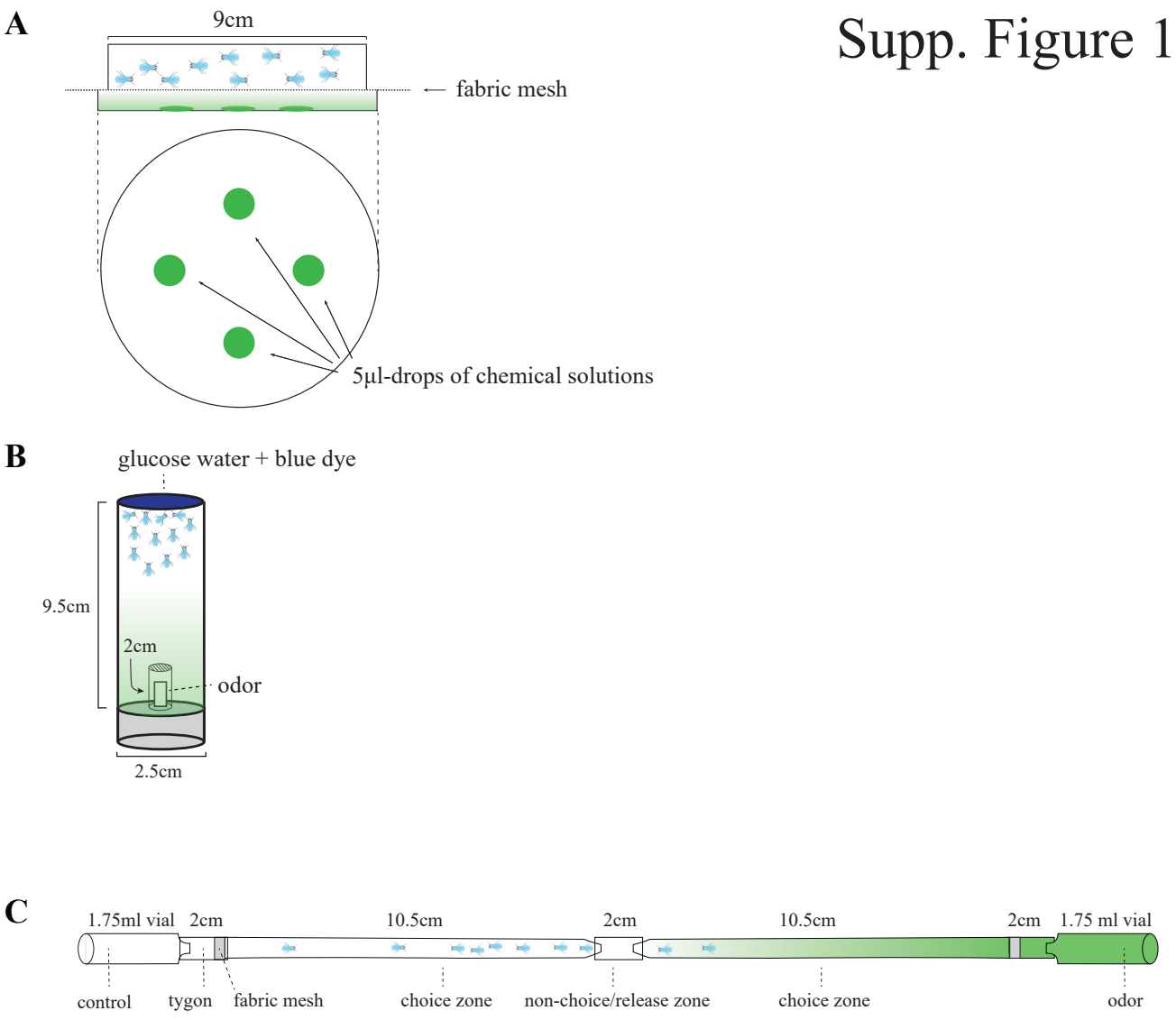

Supp.Figure 2

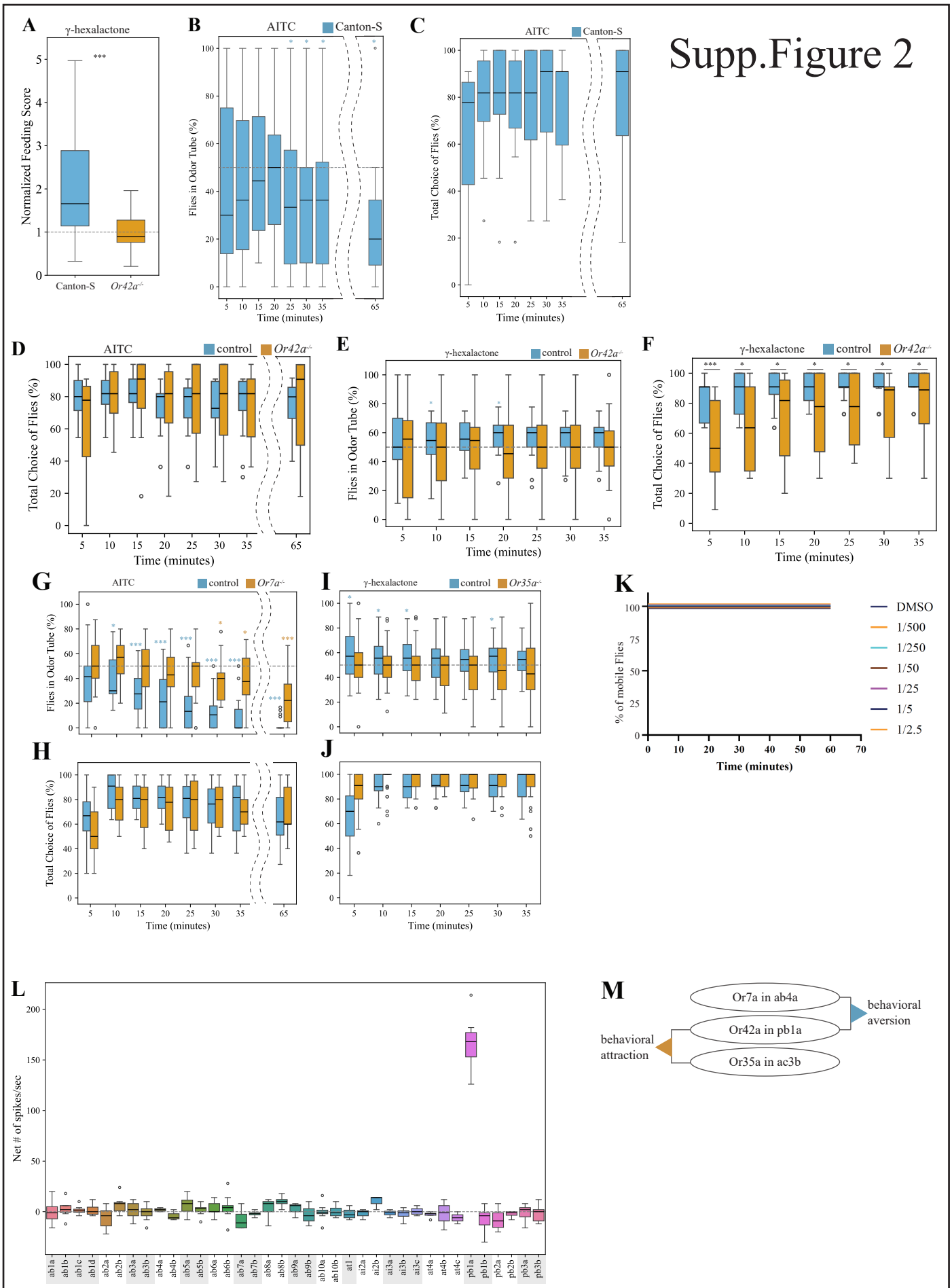

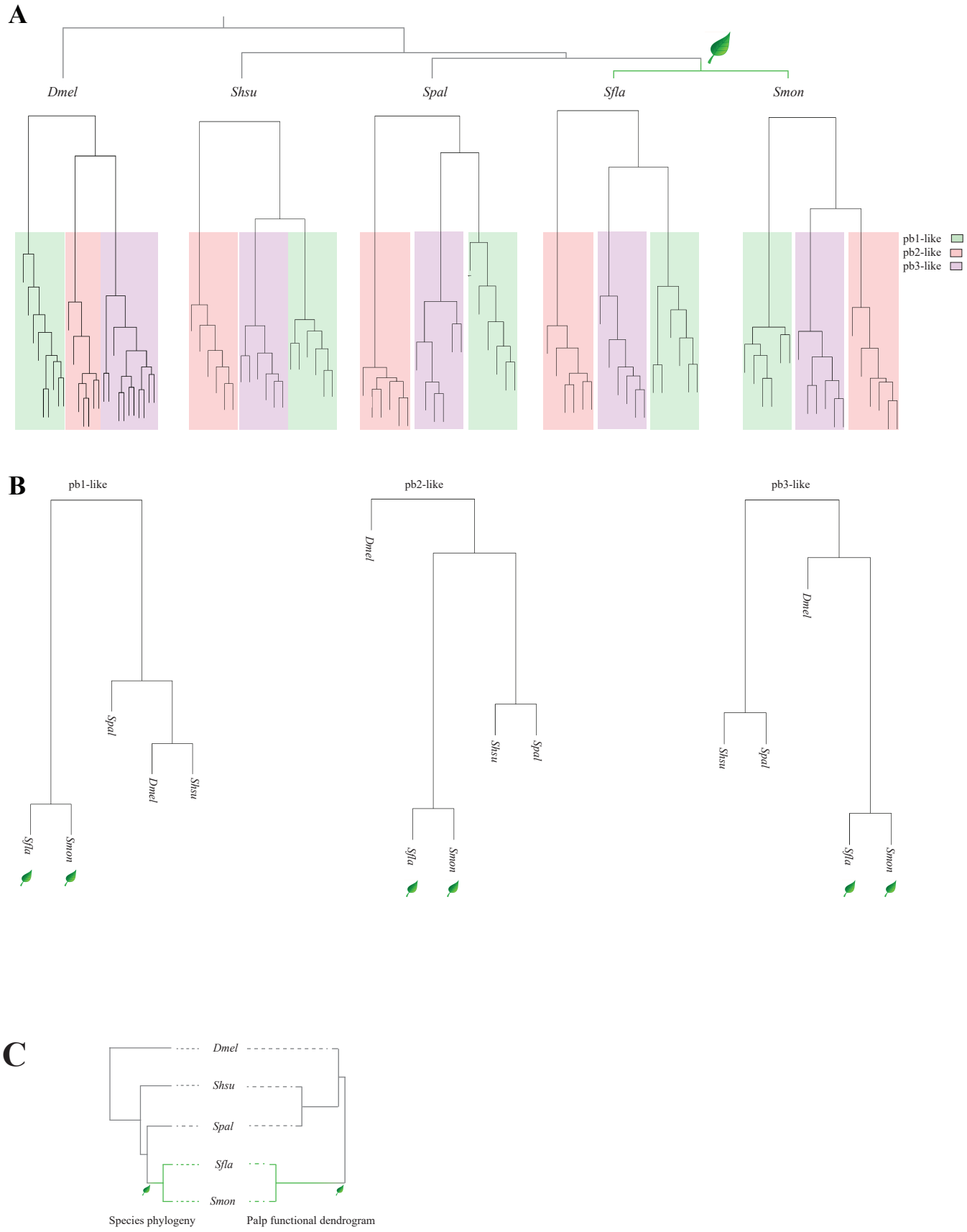

Supp. Figure 3

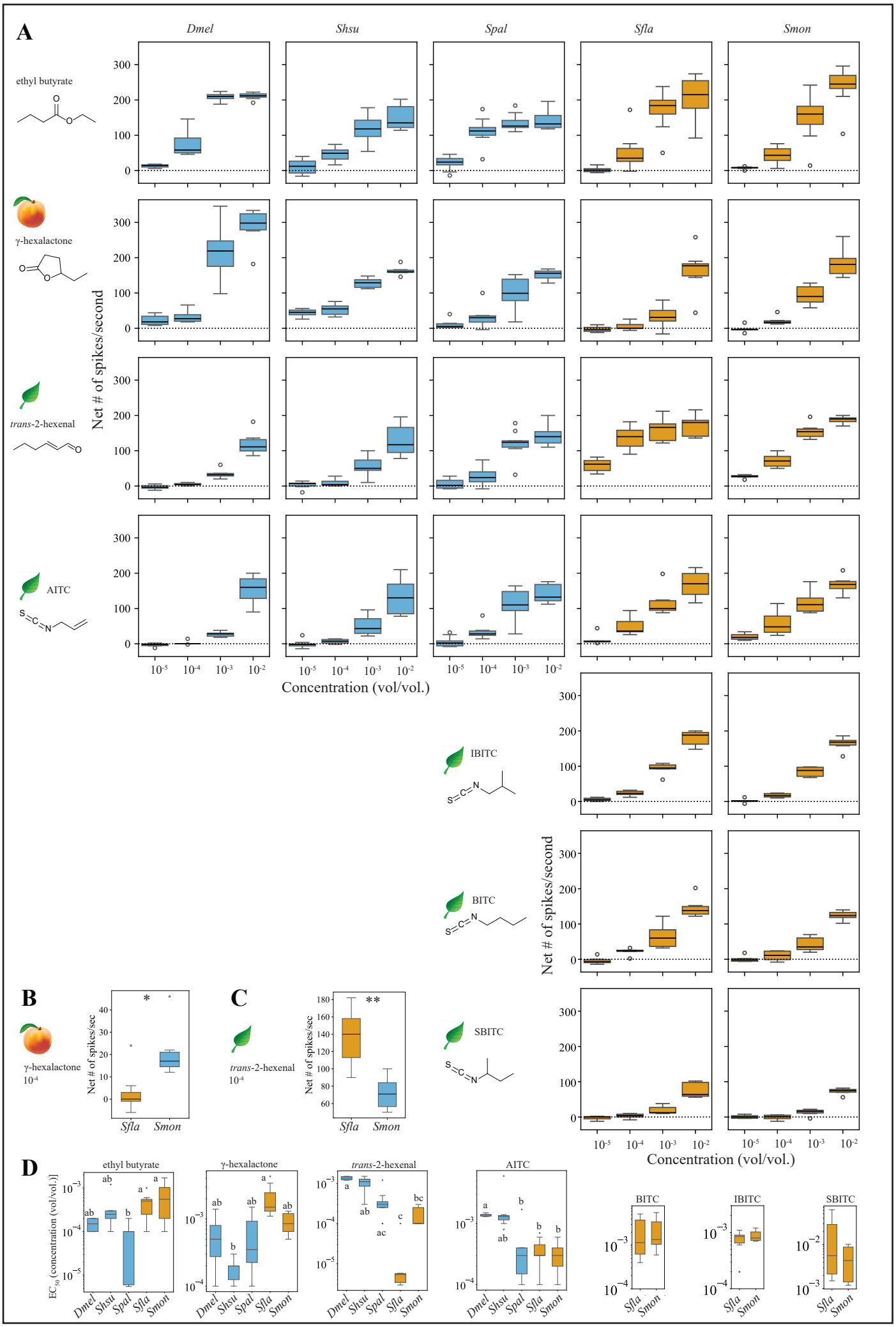
A
Dmel
Shsu
Spal
Sfla
Smon
ethyl butyrate
γ-hexalactone
trans-2-hexenal
AITC
IBITC
BITC
SBITC
Net # of spikes/second
Concentration (vol/vol.)
B
γ-hexalactone
10-4
Net # of spikes/sec
Sfla
Smon
C
trans-2-hexenal
10-4
Net # of spikes/sec
D
ethyl butyrate
γ-hexalactone
trans-2-hexenal
AITC
BITC
IBITC
SBITC
EC50 (concentration (vol/vol.))

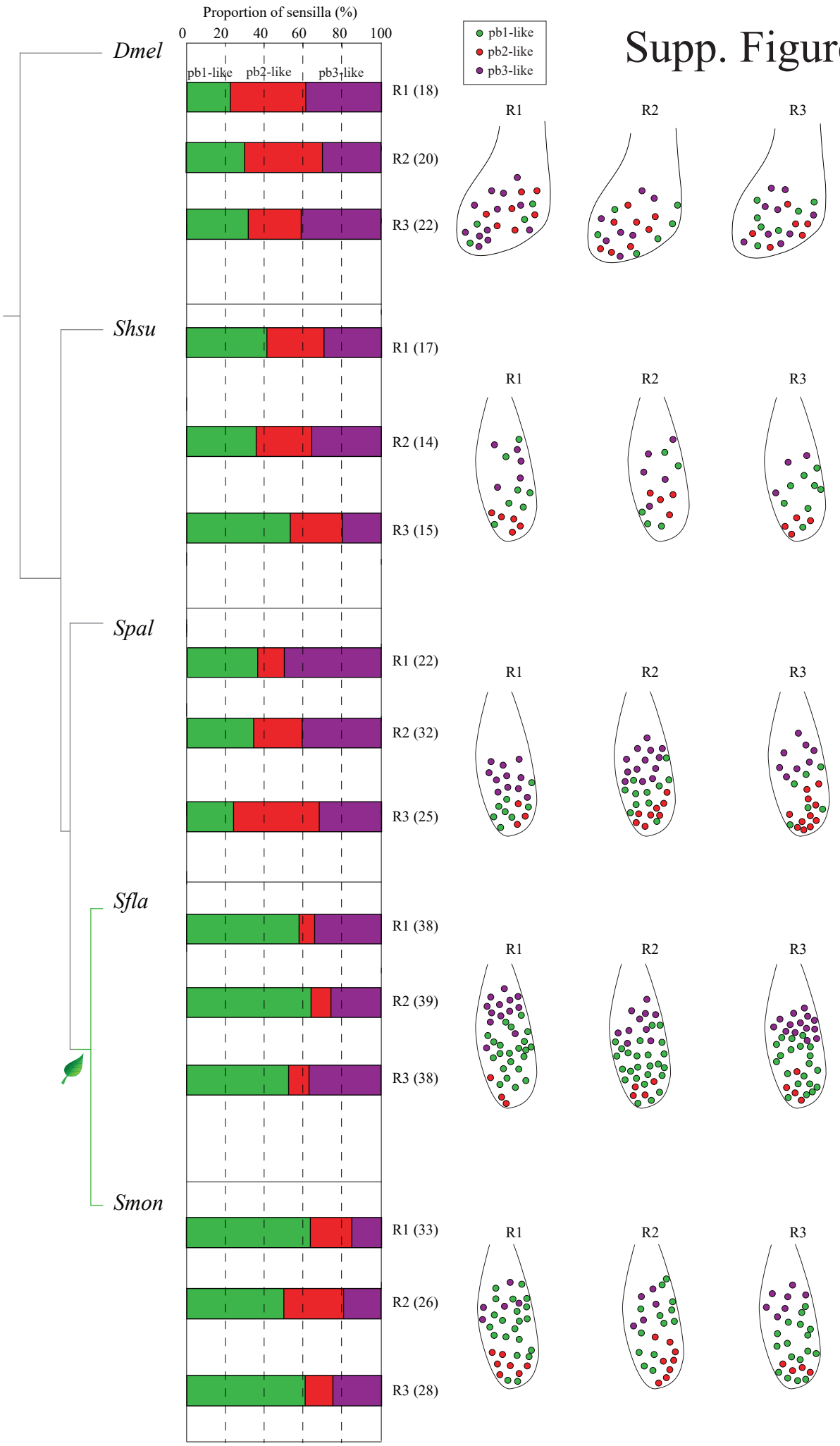
Supp. Figure 5
Proportion of sensilla (%)
0
20
40
60
80
100
pb1-like
pb2-like
pb3-like
Dmel
R1 (18)
R2 (20)
R3 (22)
Shsu
R1 (17)
R2 (14)
R3 (15)
Spal
R1 (22)
R2 (32)
R3 (25)
Sfla
R1 (38)
R2 (39)
R3 (38)
Smon
R1 (33)
R2 (26)
R3 (28)
R1
R2
R3

Supp. Figure 6

A

B

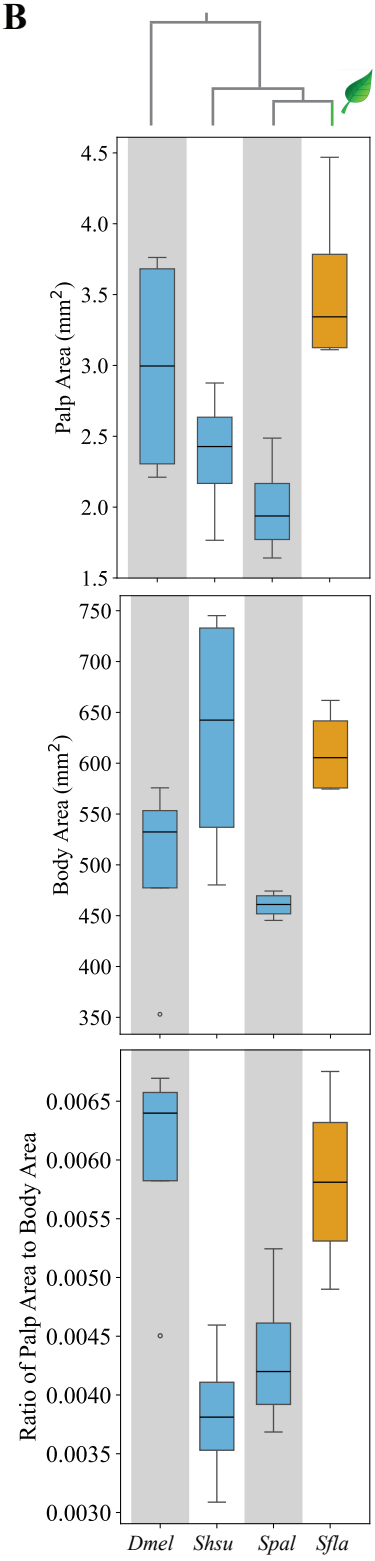

Supp. Figure 7

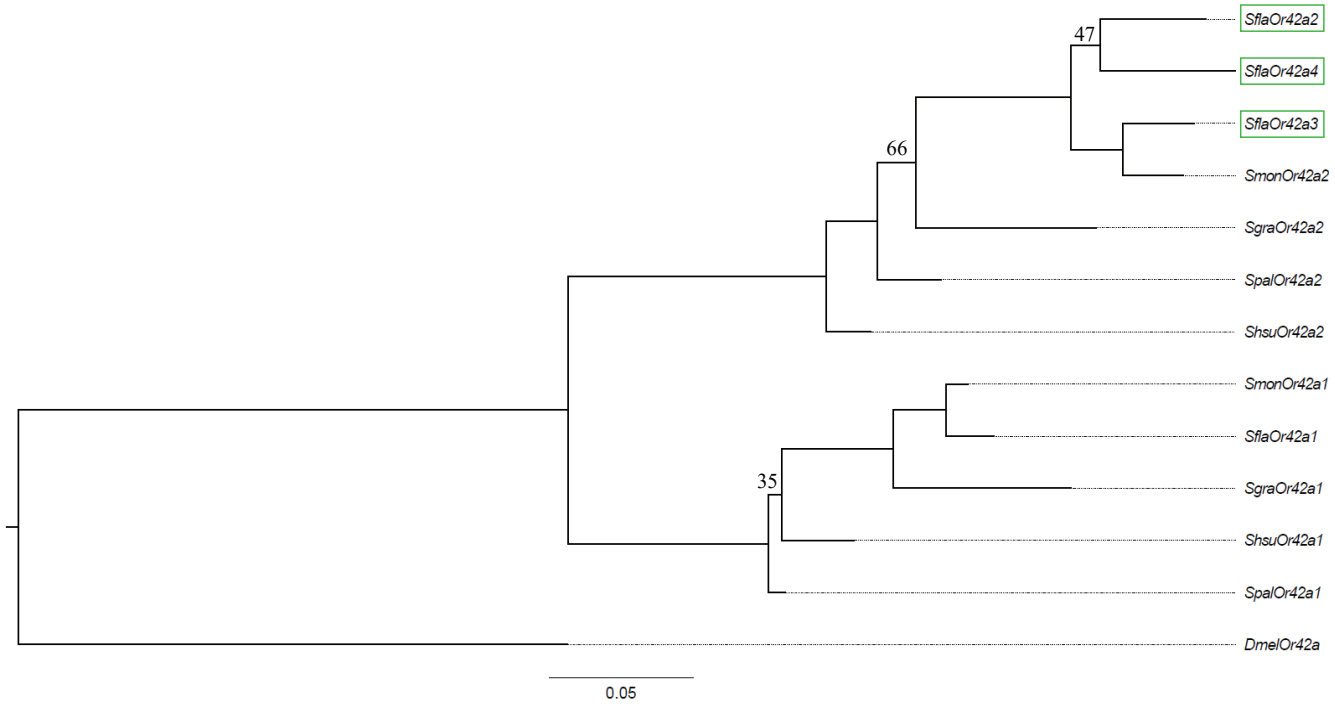

Supp. Figure 8

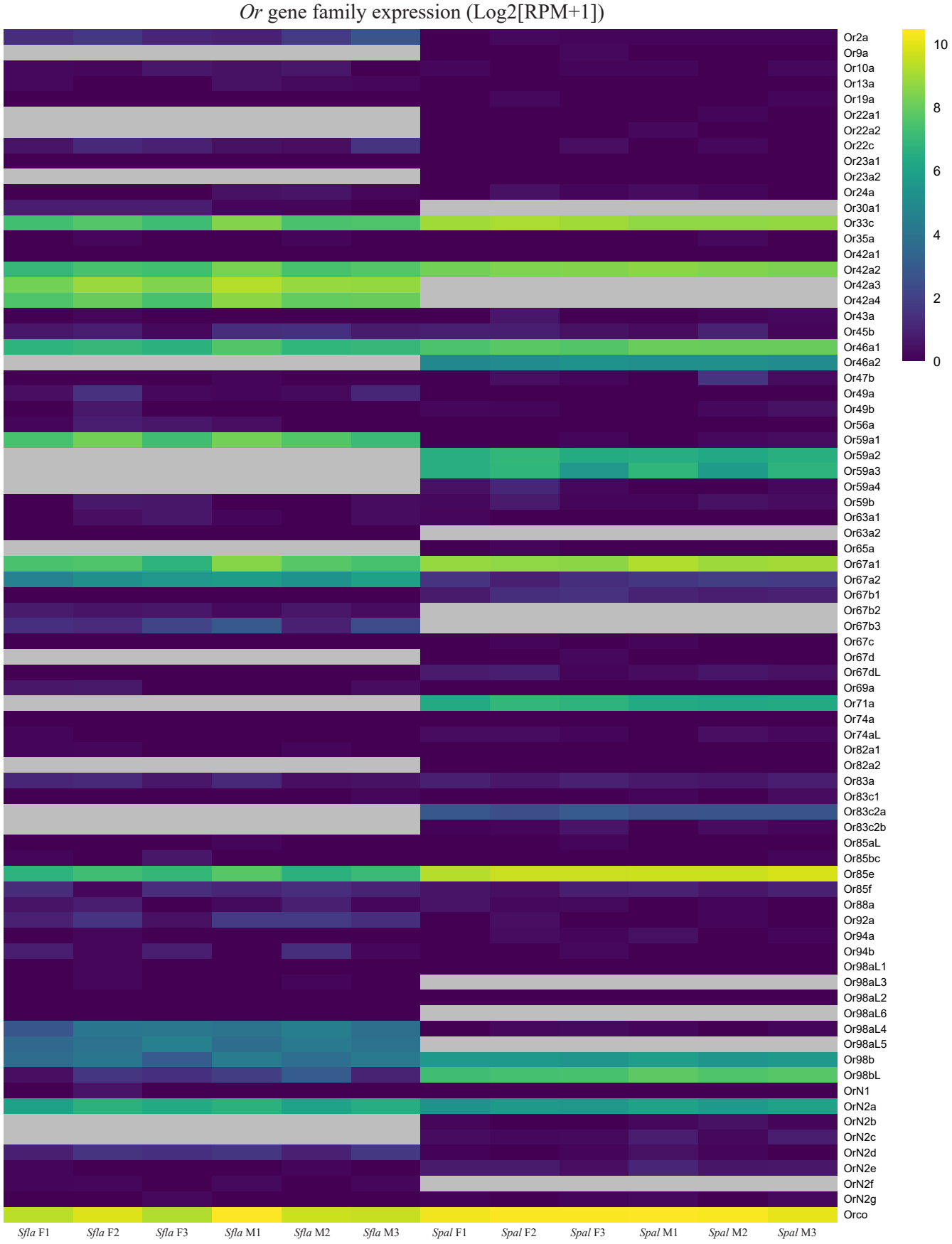

Sup. Figure 9

A

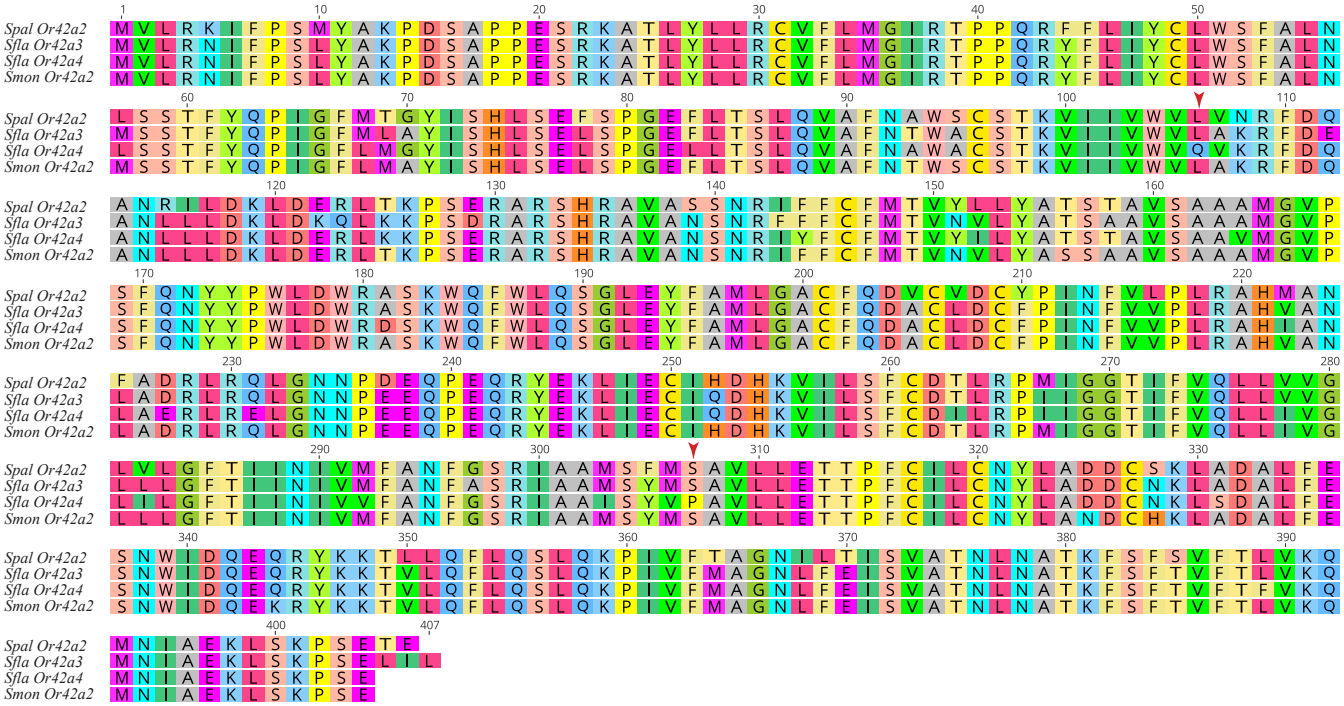

B

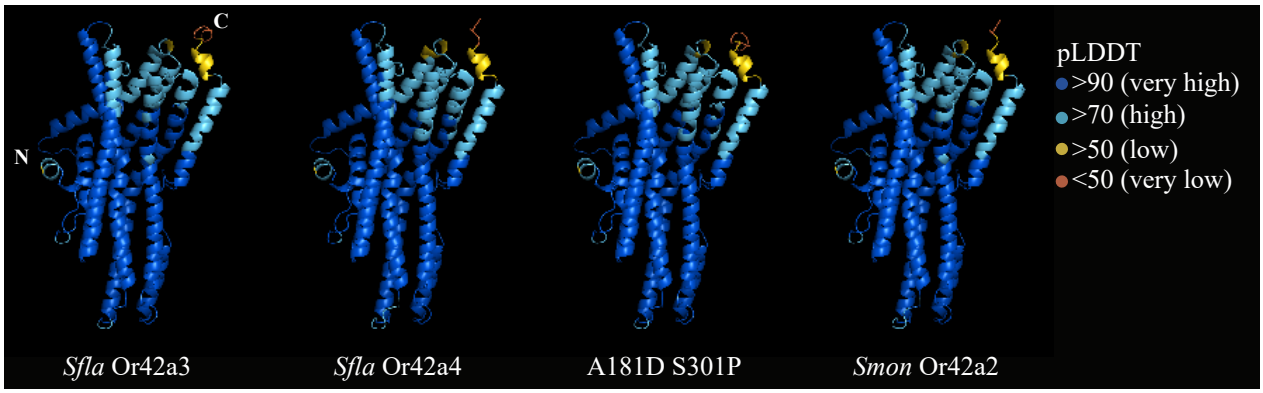

Supp. Figure 10

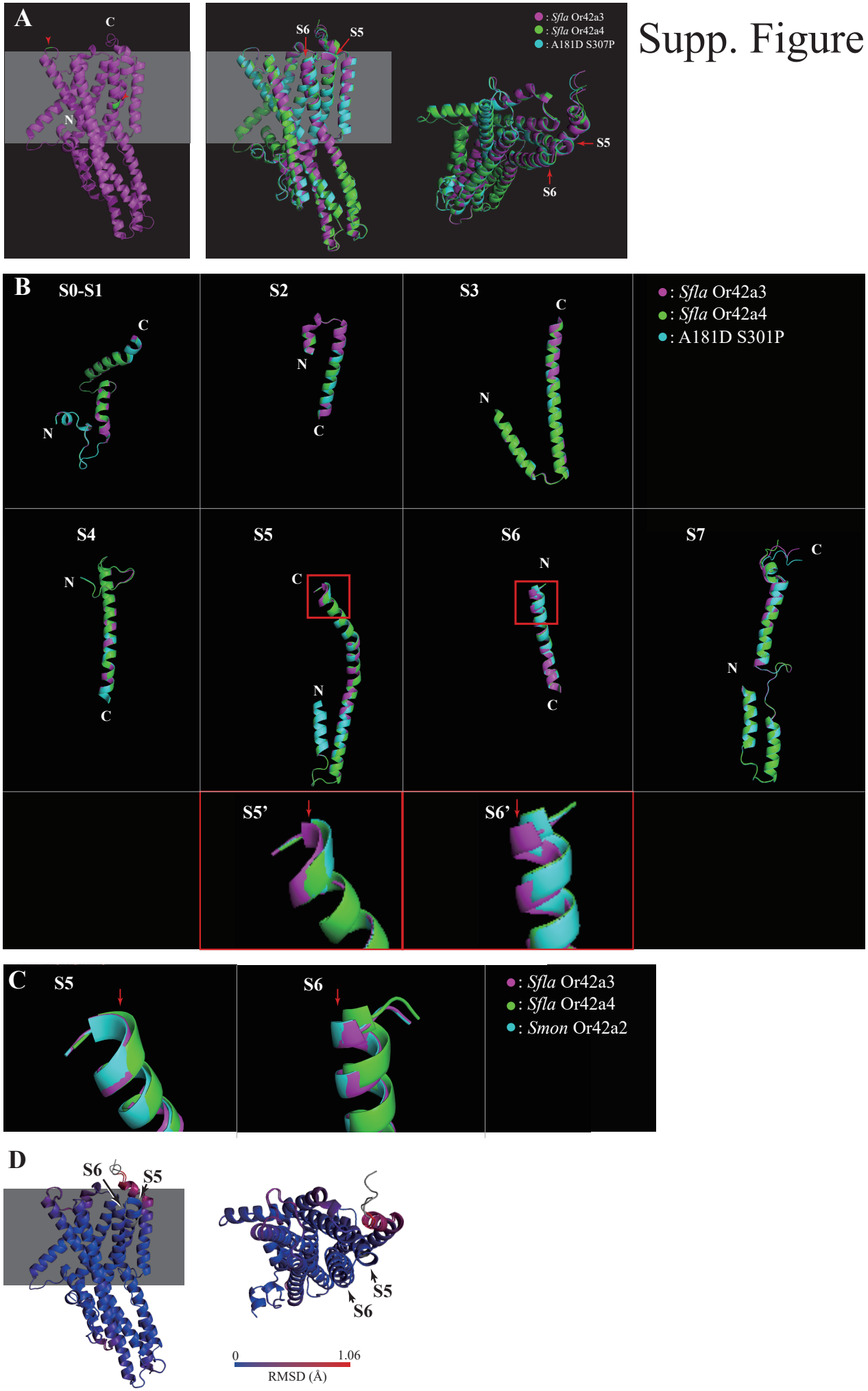

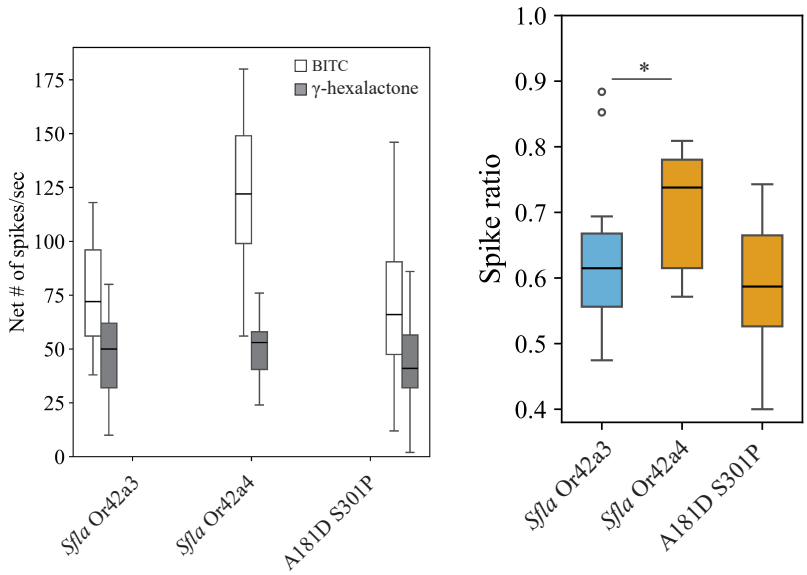

Supp. Figure 11
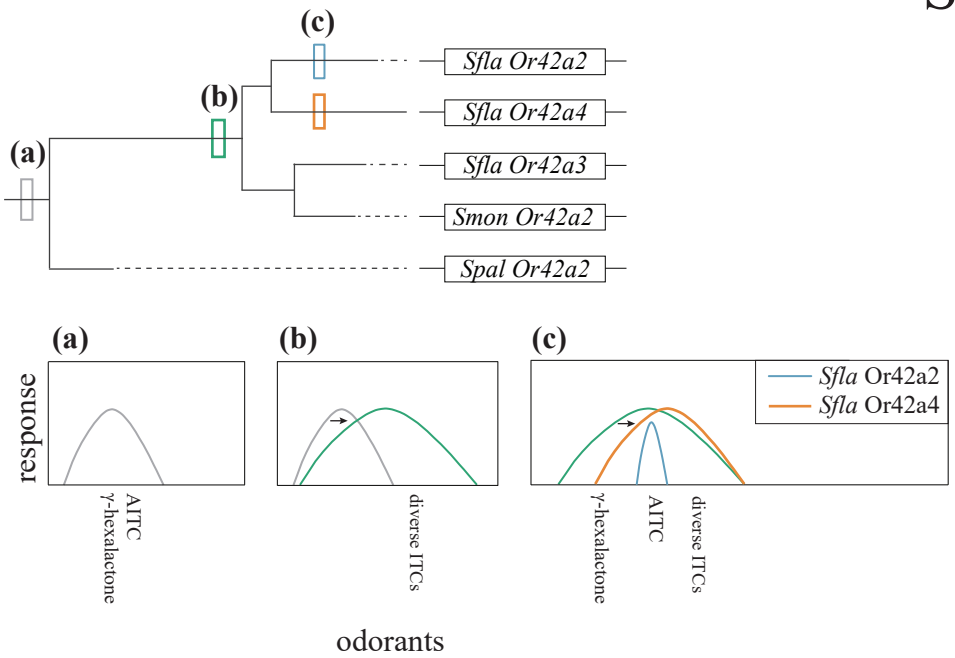
Supp. Figure 12